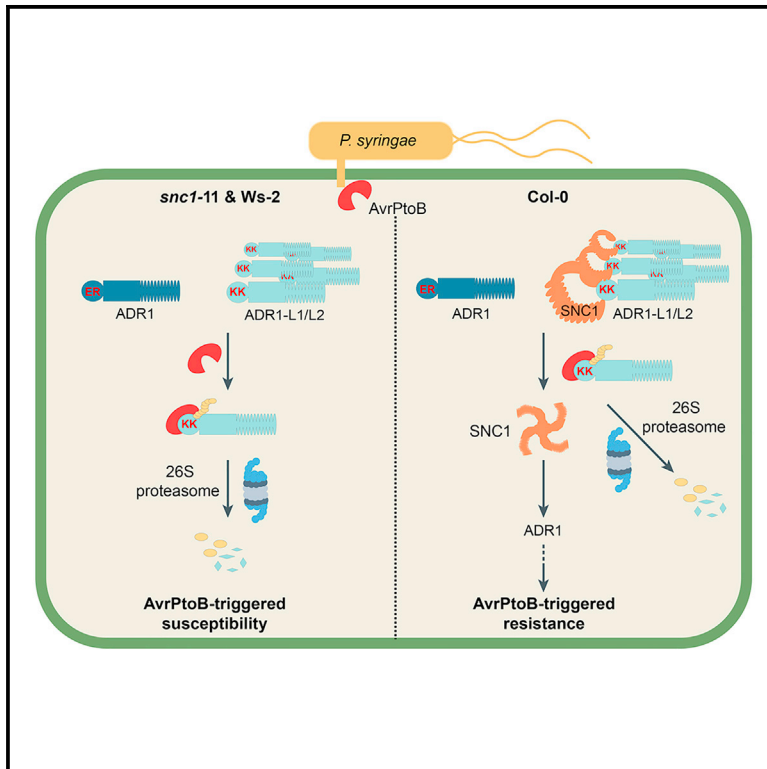


# Cell Host & Microbe

## The plant immune receptor SNC1 monitors helper NLRs targeted by a bacterial effector

### Graphical abstract



### Authors

Ming-Yu Wang, Jun-Bin Chen,  
Rui Wu, ..., Detlef Weigel,  
Jian-Hua Huang, Wang-Sheng Zhu

### Correspondence

jianhua.huang@tsl.ac.uk (J.-H.H.),  
wangshengzhu@cau.edu.cn (W.-S.Z.)

### In brief

Helper NLRs ADR1s are central components of plant immunity. Wang et al. show that bacterial effector AvrPtoB degrades ADR1-L1 and ADR1-2. ADR1 evades such degradation by diversifying the ubiquitination sites of AvrPtoB. Disruption of ADR1-L1/L2 activates their guarding sensor NLR SNC1, which signals through ADR1 to trigger immune responses.

### Highlights

- Effector AvrPtoB degrades helper NLRs ADR1-L1/L2, but not ADR1
- Mutation in *SNC1* abolishes the autoimmunity of the *adr1-L1* null mutants
- Delivery of AvrPtoB or loss of *ADR1-L1* triggers the oligomerization of SNC1
- SNC1 guards ADR1-L1/L2 and signals through ADR1



## Article

# The plant immune receptor SNC1 monitors helper NLRs targeted by a bacterial effector

Ming-Yu Wang,<sup>1,7</sup> Jun-Bin Chen,<sup>1,7</sup> Rui Wu,<sup>2,7,8</sup> Hai-Long Guo,<sup>4,7</sup> Yan Chen,<sup>1</sup> Zhen-Ju Li,<sup>1</sup> Lu-Yang Wei,<sup>1</sup> Chuang Liu,<sup>1</sup> Sheng-Feng He,<sup>1</sup> Mei-Da Du,<sup>1</sup> Ya-long Guo,<sup>5</sup> You-Liang Peng,<sup>4</sup> Jonathan D.G. Jones,<sup>3</sup> Detlef Weigel,<sup>2,6</sup> Jian-Hua Huang,<sup>3,\*</sup> and Wang-Sheng Zhu<sup>1,9,\*</sup>

<sup>1</sup>Key Laboratory of Surveillance and Management for Plant Quarantine Pests, Ministry of Agriculture and Rural Affairs, and College of Plant Protection, State Key Laboratory of Maize Bio-breeding, China Agricultural University, Beijing 100193, China

<sup>2</sup>Department of Molecular Biology, Max Planck Institute for Biology Tübingen, 72076 Tübingen, Germany

<sup>3</sup>The Sainsbury Laboratory, University of East Anglia, Norwich Research Park, Norwich NR4 7UH, UK

<sup>4</sup>Key Laboratory of Pest Monitoring and Green Management, Ministry of Agriculture and Rural Affairs, and College of Plant Protection, China Agricultural University, Beijing 100193, China

<sup>5</sup>State Key Laboratory of Systematic and Evolutionary Botany, Institute of Botany, Chinese Academy of Sciences, Beijing 100093, China

<sup>6</sup>Institute for Bioinformatics and Medical Informatics, University of Tübingen, Tübingen, Germany

<sup>7</sup>These authors contributed equally

<sup>8</sup>Present address: Department of Plant & Environmental Studies, Copenhagen University, 1871 Frederiksberg, Denmark

<sup>9</sup>Lead contact

\*Correspondence: [jianhua.huang@tsl.ac.uk](mailto:jianhua.huang@tsl.ac.uk) (J.-H.H.), [wangshengzhu@cau.edu.cn](mailto:wangshengzhu@cau.edu.cn) (W.-S.Z.)

<https://doi.org/10.1016/j.chom.2023.10.006>

## SUMMARY

Plants deploy intracellular receptors to counteract pathogen effectors that suppress cell-surface-receptor-mediated immunity. To what extent pathogens manipulate intracellular receptor-mediated immunity, and how plants tackle such manipulation, remains unknown. *Arabidopsis thaliana* encodes three similar ADR1 class helper nucleotide-binding domain leucine-rich repeat receptors (ADR1, ADR1-L1, and ADR1-L2), which are crucial in plant immunity initiated by intracellular receptors. Here, we report that *Pseudomonas syringae* effector AvrPtoB suppresses ADR1-L1- and ADR1-L2-mediated cell death. ADR1, however, evades such suppression by diversifying into two ubiquitination sites targeted by AvrPtoB. The intracellular sensor SNC1 interacts with and guards the CC<sub>R</sub> domains of ADR1-L1/L2. Removal of ADR1-L1/L2 or delivery of AvrPtoB activates SNC1, which then signals through ADR1 to trigger immunity. Our work elucidates the long-sought-after function of SNC1 in defense, and also how plants can use dual strategies, sequence diversification, and a multi-layered guard-guardee system, to counteract pathogen's attack on core immunity functions.

## INTRODUCTION

Plants are constantly threatened by pathogens. To impede pathogen invasion, plants deploy plasma-membrane-localized pattern-recognition receptors (PRRs) that initiate pattern-triggered immunity (PTI) upon detection of conserved molecular patterns diagnostic of pathogens. To enable successful invasion, pathogens in turn deliver effectors into plant cells to manipulate components of PTI. To antagonize the action of effectors, plants evolved intracellular nucleotide-binding domain leucine-rich repeat receptors (NLRs), which detect effectors or their effects on host proteins. The outcome is an enhanced immune response known as effector-triggered immunity (ETI). ETI usually culminates in programmed cell death called hypersensitive response (HR), a hallmark of ETI.<sup>1,2</sup> Recent studies have revealed at the molecular level how PTI and ETI are interlinked, with PTI and ETI potentiating each other.<sup>3–6</sup>

NLRs are classified into TIR-NLRs (TNLs), CC-NLRs (CNLs), and CC<sub>R</sub>-NLRs (RNLs), based on their N termini. RNLs are considered to function as helper NLRs downstream of sensor NLRs including most TNLs and some CNLs, which can directly or indirectly recognize effectors. Helper NLRs are encoded by three gene families, each with a different founding member: *ADR1* (*ACTIVATED DISEASE RESISTANCE 1*), *NRG1* (*N REQUIREMENT GENE 1*), and *NRC* (*NLR PROTEIN REQUIRED FOR HYPERSENSITIVE-RESPONSE-ASSOCIATED CELL DEATH*). ADR1 homologs are ubiquitously present in angiosperm genomes, whereas the NRG1 and NRC families are limited to dicots and Solanaceae, respectively.<sup>7</sup> The *Arabidopsis thaliana* genome encodes three unequally members of the ADR1 family: including ADR1, ADR1-L1, and ADR1-L2.<sup>7</sup> Similar to activated ZAR1 and Sr35 as well as NRG1, autoactive ADR1 can form Ca<sup>2+</sup>-permeable influx channels that activate cell death.<sup>8–10</sup> In addition, ADR1s form complexes with EDS1 (*ENHANCED DISEASE SUSCEPTIBILITY 1*)-PAD4 (*PHYTOALEXIN DEFICIENT 4*) heterodimers.<sup>3,11</sup> Similar to the



*eds1* mutant, *adr1 adr1-L1 adr1-L2* triple mutants are highly susceptible to virulent *Pseudomonas syringae* and to avirulent pathogens, resistance to which relies primarily on not only TNLs but also some CNLs.<sup>12,13</sup> EDS1-PAD4-ADR1 complexes are also required for full PTI responses triggered by elicitor nlp20.<sup>3,6</sup> Taken together, these findings suggest that ADR1s play a key role in ETI and PTI.

*SNC1* (*SUPPRESSOR OF NPR1-1, CONSTITUTIVE 1*) encodes an extensively studied canonical sensor TNL.<sup>14</sup> Overexpression of wild-type *SNC1* activates salicylic acid (SA)-dependent defense responses,<sup>15</sup> and a gain-of-function mutation in the coding sequence can suppress disease susceptibility of *npr1-1* mutants, which are defective in systemic acquired resistance (SAR).<sup>14,16</sup> Subsequent studies on *SNC1* uncovered complex control of NLRs, including epigenetic regulation, alternative splicing, intracellular trafficking, post-translational modification, and structural variation at *SNC1* itself.<sup>17,18</sup> Inactivation of *SNC1* restores elevated disease resistance seen in a range of autoimmune mutants with defects in very different types of genes.<sup>17</sup> Remarkably, although *SNC1* has become a powerful model to understand many different aspects of the regulation of NLR activity, its physiological roles in plant immunity, if any, has remained elusive.

An important role of pathogen effectors is to antagonize PTI components, with some type III secretion system (T3SS) effectors of *P. syringae* also suppressing ETI by mechanisms that have so far been unknown.<sup>19–21</sup> For example, HopI1 greatly dampens HR triggered by several other effectors.<sup>21</sup> A recent reverse genetic screen identified five effectors from oomycetes and nematodes that suppress cell death triggered by NLRs Prf or Rpi-blb2 in *Nicotiana benthamiana*.<sup>22</sup> Among these effectors, SS15 exerts its effects by inhibiting the intramolecular rearrangements of NRC2, which prevents its oligomerization and activation,<sup>23</sup> whereas AVRcap1b dampens NRC2 and NRC3 function through the membrane trafficking-associated protein NbTOL9a (target of Myb 1-like protein 9a).<sup>22</sup> From these studies, it is clear that much is still to be learned about how pathogens suppress ETI and how plants in turn counteract such suppression.

We report that the *P. syringae* effector AvrPtoB, an E3 ligase, ubiquitinates and thereby promotes degradation of the *A. thaliana* helper NLR ADR1-L1, which in turn induces oligomerization of the sensor NLR SNC1, an ADR1-L1 guard. Two non-synonymous substitutions in the CC<sub>R</sub> domain allow the ADR1-L1 homolog ADR1 to evade AvrPtoB-mediated ubiquitination. The autoimmunity of *adr1-L1-c1* single and *adr1-L1-c1 adr1-L2* double mutants are suppressed by the inactivation of ADR1, indicating that ADR1 acts downstream of ADR1-L1 and ADR1-L2. Together, we demonstrate that the sensor NLR SNC1 recognizes AvrPtoB by guarding ADR1-L1 and ADR1-L2, then signals through ADR1 for immune responses. Our findings uncover a plant mechanism for counteracting ETI suppression by bacterial effectors, illustrating yet another layer of the mechanisms by which plants neutralize pathogen effectors.

## RESULTS

### AvrPtoB induces ADR1-L1 protein degradation

We use the *Pseudomonas syringae* pv. tomato (*Pst*) DC3000 model pathogen to study interactions between the plant immune system and bacterial effectors. To identify *Pst* DC3000 effectors that suppress the activity of the essential ETI component ADR1-

L1 from *A. thaliana* (hereafter Arabidopsis), we first generated an autoactive ADR1-L1 variant (ADR1-L1<sup>D489V</sup>), which triggers robust cell death in *N. benthamiana* (Figure S1A). We co-expressed this variant, with a mutation in the MHD regulatory motif, in individual combinations with 31 of the 36 *Pst* DC3000 effectors in *N. benthamiana* in search for effectors that might dampen ADR1-L1<sup>D489V</sup>-triggered cell death (Figure 1A). Only AvrPtoB did so completely (Figures 1B and S1B).

AvrPtoB is a U-box E3 ligase.<sup>24</sup> The E3 ligase-dead variant AvrPtoB<sup>F173A/F479A</sup> (Janjusevic et al.<sup>24</sup>) did not suppress ADR1-L1<sup>D489V</sup>-triggered cell death (Figure 1B), indicating that AvrPtoB uses its E3 ligase activity to manipulate ADR1-L1 function. Levels of ADR1-L1-FLAG protein in *N. benthamiana* leaves were substantially reduced when co-expressed with AvrPtoB-HA, but not when co-expressed with the catalytically inactive AvrPtoB<sup>F173A/F479A</sup> variant (Figure 1C). Such reduction was alleviated in the presence of the 26S proteasome inhibitor MG132, but not in the presence of BAF (Bafilomycin A1), which inhibits protein degradation by the autophagy pathway (Figure 1D). These results suggest that AvrPtoB triggers ADR1-L1 degradation in an E3 ligase activity-dependent manner via the 26S proteasome pathway.

To further confirm that degradation of ADR1-L1 can be catalyzed by AvrPtoB, wild-type and catalytically inactive variants of AvrPtoB were delivered by the effectorless *Pst* DC3000 D36E strain<sup>19</sup> into Arabidopsis *ADR1-L1-FLAG-TurboID* plants. The level of ADR1-L1-FLAG-TurboID protein had increased at 3 h post-infiltration (hpi) for all treatments (Figure 1E), likely due to the activation of PTI by *Pst* DC3000 D36E. ADR1-L1-FLAG-TurboID protein level increases had leveled off at 6 hpi when plants were infiltrated with *Pst* DC3000 D36E expressing AvrPtoB, decreasing further at 12 hpi (Figure 1E). In contrast, no changes in ADR1-L1-FLAG-TurboID protein level were observed at 6 and 12 hpi when plants were infiltrated with *Pst* DC3000 D36E expressing AvrPtoB<sup>F173A/F479A</sup> (Figure 1E). Taken together, these observations suggest that AvrPtoB can induce the degradation of ADR1-L1 in Arabidopsis after pathogen infection.

### The CC<sub>R</sub> domain determines AvrPtoB target specificity

Since the three ADR1 members share similar functions in regulating intracellular receptor-dependent immune responses, we wondered whether AvrPtoB also compromised the stability of ADR1 and ADR1-L2 as well as the ability of their autoactive variants to trigger HR. In contrast to ADR1-L1<sup>D489V</sup>, HR triggered by ADR1<sup>D461V</sup> was only rarely suppressed, and HR triggered by ADR1-L2<sup>D484V</sup> was only slightly suppressed by AvrPtoB (Figure 2A), although the co-immunoprecipitation (coIP) and split-luciferase complementation (SLC) experiments had indicated that AvrPtoB can interact with all ADR1 homologs (Figures 2B, S2A, and S2B). In agreement, ADR1 protein levels in *N. benthamiana* were not affected by AvrPtoB (Figure S2C). The weak effects on ADR1-L2 protein abundance may be due to mild suppression of ADR1-L2 activity by AvrPtoB, consistent with the modest impairment of ADR1-L2<sup>D484V</sup>-mediated cell death by AvrPtoB (Figures 2A and S2C). *Pst* DC3000 D36E carrying AvrPtoB did not alter the protein level of either ADR1-FLAG-TurboID or ADR1-L2-FLAG-TurboID in Arabidopsis (Figure S2D).

Ubiquitination occurs on lysine residues, and since the TurboID tag can cause biotinylation on lysine residues, this might interfere with AvrPtoB-mediated degradation and lead to differential

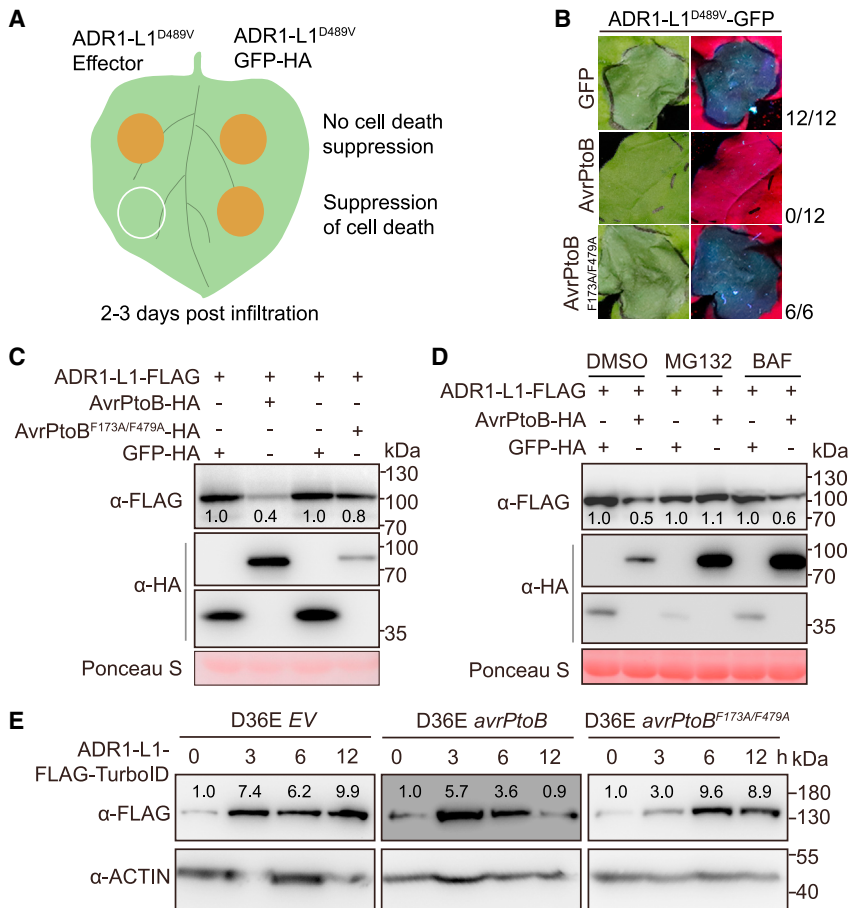


**Figure 1. AvrPtoB suppresses ADR1-L1-triggered HR and induces the degradation of ADR1-L1**

(A) Schematic diagram of the screen for *Pst* DC3000 effectors that suppress HR triggered by transient expression of ADR1-L1<sup>D489V</sup> in *N. benthamiana*. (B) E3 ligase activity of AvrPtoB is required for suppression of HR triggered by ADR1-L1<sup>D489V</sup>. Numbers on the far right indicate leaves showing obvious HR over all infiltrated leaves. (C) E3 ligase activity is required for AvrPtoB inducing degradation of ADR1-L1. (D) The 26S proteasome inhibitor MG132 blocks degradation of ADR1-L1 induced by AvrPtoB. (E) AvrPtoB induces degradation of ADR1-L1-FLAG-TurboID in 4-week-old transgenic Arabidopsis plants. Rosette leaves plants were infiltrated with *Pst* D36E EV, *Pst* D36E *avrPtoB*, or *Pst* D36E *avrPtoB*<sup>F173A/F479A</sup> (OD<sub>600</sub> = 0.4) and collected for immunoblots in at 0, 3, 6, and 12 hpi. Numbers indicate arbitrary densitometric units of bands after normalization to the left-most ADR1-L1-FLAG-TurboID band of each immunoblot. Experiments were performed three times, with similar results. See also Figure S1 and Table S1.

**Two lysine residues in the CC<sub>R</sub> domain enable evasion of AvrPtoB-mediated ubiquitination**

As sequence differences in the CC<sub>R</sub> domains are responsible for differential effects of AvrPtoB on ADR1 homologs, we tested whether AvrPtoB can inhibit also the cell death caused by transient expres-

degradation of ADR1 homologs by AvrPtoB. We thus tested if ADR1s tagged with FLAG-TurboID were biotinylated in Arabidopsis. As shown in Figure S1C, only a small amount of any of the ADR1s tagged with FLAG-TurboID was biotinylated in the absence of exogenous biotin. This suggests that the differential degradation of ADR1s tagged with FLAG-TurboID (Figures 1E and S2D) is unlikely to be due to biotinylation of ADR1s. Instead, these results suggest that AvrPtoB affects the stability of ADR1 homologs as well as the HR they trigger in a homolog-specific manner.

To identify the causal domains responsible for differential suppression of ADR1- and ADR1-L1-triggered HR by AvrPtoB, we swapped the CC<sub>R</sub> (Coiled Coil of Resistance to Powdery Mildew Locus 8), NB (Nucleotide Binding)-ARC (Apaf1, Certain R Genes and CED4), and LRR (Leucine Rich Repeat) domains between ADR1-L1<sup>D489V</sup> and ADR1<sup>D461V</sup>. Interchange of the CC<sub>R</sub> domain, but not the NB-ARC and LRR domains, made ADR1<sup>D461V</sup>-triggered cell death responsive to AvrPtoB, and at the same time made ADR1-L1<sup>D489V</sup>-triggered cell death insensitive to AvrPtoB (Figures 2C and S2E). In agreement, ADR1<sup>D461V</sup> with the CC<sub>R</sub><sup>ADR1-L1</sup> domain, but not with the NB-ARC<sup>ADR1-L1</sup> or LRR<sup>ADR1-L1</sup> domains, accumulated to a lower level in the presence of AvrPtoB, whereas the levels of ADR1-L1<sup>D489V</sup> with the CC<sub>R</sub><sup>ADR1</sup> domain were insensitive to the presence of AvrPtoB (Figures 2D and S2F). These results indicate that the CC<sub>R</sub> domain determines the specificity of AvrPtoB-mediated suppression of ADR1-L1 activity.

sion of only the CC<sub>R</sub> domain of ADR1 homologs in *N. benthamiana*.<sup>10,25</sup> Similar to AvrPtoB effects on the autoactive full-length variants, AvrPtoB did not affect CC<sub>R</sub><sup>ADR1</sup>-triggered cell death, slightly suppressed CC<sub>R</sub><sup>ADR1-L2</sup>-triggered cell death, and abolished CC<sub>R</sub><sup>ADR1-L1</sup>-triggered cell death (Figure 3A). This was paralleled by AvrPtoB having little impact on the protein levels of CC<sub>R</sub><sup>ADR1</sup> and CC<sub>R</sub><sup>ADR1-L2</sup> but causing a substantial reduction of CC<sub>R</sub><sup>ADR1-L1</sup> levels (Figure S3A). Thus, the effects of AvrPtoB on both protein accumulation and cell-death-inducing ability are similar between the CC<sub>R</sub> domains and full-length ADR1 homologs (Figures 2A, 3A, S2C, and S3A).

Because the MBP-tagged CC<sub>R</sub> domains of all three ADR1 homologs were similarly pulled down by purified GST-AvrPtoB, interaction of AvrPtoB with CC<sub>R</sub> domains (Figure 3B) is apparently not sufficient for AvrPtoB to promote protein degradation (Figure S3A), likely due to differential ubiquitination of CC<sub>R</sub><sup>ADR1</sup> and CC<sub>R</sub><sup>ADR1-L1</sup> by AvrPtoB. An *in vitro* assay confirmed that AvrPtoB can ubiquitinate CC<sub>R</sub><sup>ADR1-L1</sup> and CC<sub>R</sub><sup>ADR1-L2</sup> but not CC<sub>R</sub><sup>ADR1</sup> (Figure 3C). This is consistent with AvrPtoB being able to at least partially suppress cell death triggered by CC<sub>R</sub><sup>ADR1-L1</sup> and CC<sub>R</sub><sup>ADR1-L2</sup> and CC<sub>R</sub><sup>ADR1</sup> being immune to AvrPtoB. Our results indicate that CC<sub>R</sub><sup>ADR1</sup> escapes suppression of AvrPtoB by evading AvrPtoB-catalyzed ubiquitination.

To identify the residues that allow CC<sub>R</sub><sup>ADR1</sup> to avoid becoming ubiquitinated, we generated chimeric CC<sub>R</sub> proteins by swapping the first 50 amino acids between CC<sub>R</sub><sup>ADR1-L1</sup> and CC<sub>R</sub><sup>ADR1</sup>, then

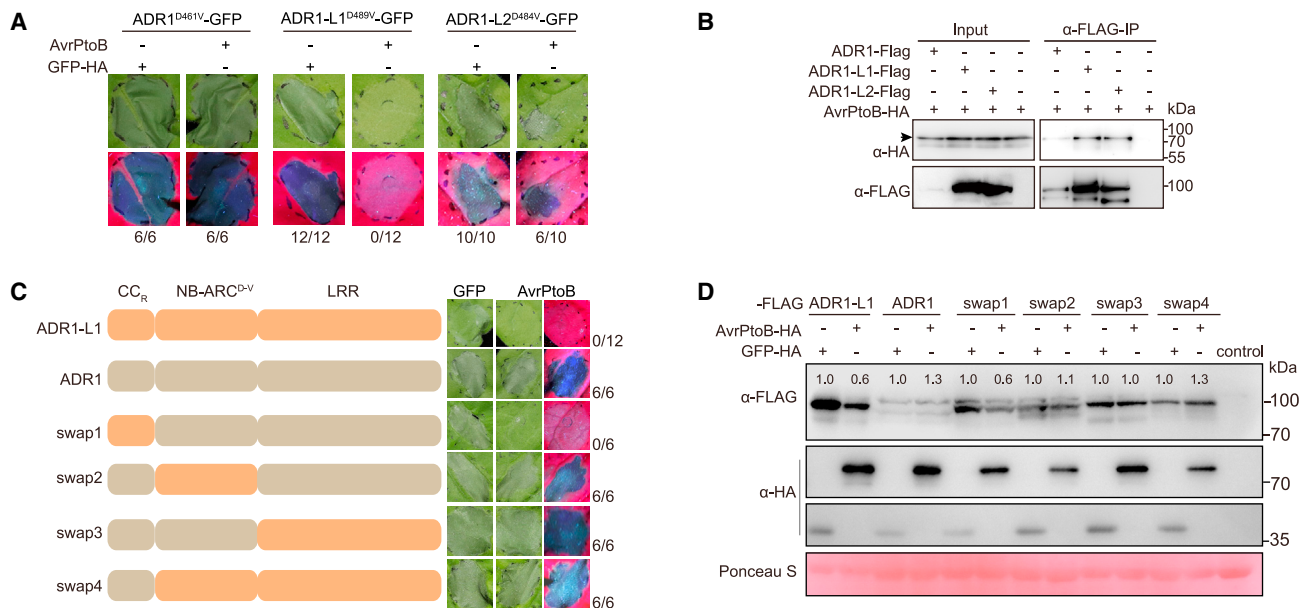


**Figure 2. The CC<sub>R</sub> domains are responsible for differential suppression of ADR1 and ADR1-L1 activity by AvrPtoB**

(A) AvrPtoB differentially suppresses HR triggered by autoactivate ADR1 homologs. ADR1<sup>D461V</sup>, ADR1-L1<sup>D489V</sup>, and ADR1-L2<sup>D484V</sup> were transiently co-expressed with GFP-HA and AvrPtoB-HA in *N. benthamiana*.

(B) AvrPtoB associates with all three ADR1 homologs, as shown by coIP in *N. benthamiana*.

(C) Domain swapping identifies the CC<sub>R</sub> domains of ADR1 homologs as determinants of susceptibility to AvrPtoB suppression. See also Figure S2E.

(D) Swapping the CC<sub>R</sub> domains between ADR1 and ADR1-L1 switches the AvrPtoB-susceptibility of ADR1 and ADR1-L1. See also Figure S2F. Numbers on the bottom (A) or far right (C) indicate leaves with HR over all infiltrated leaves. Experiments were performed three times, with similar results. See also Figure S2.

co-expressed the chimeric CC<sub>R</sub> proteins with AvrPtoB in *N. benthamiana* (Figures S3B and S3C). Although AvrPtoB failed to suppress cell death triggered by wild-type CC<sub>R</sub><sup>ADR1</sup>, it abolished the cell death caused by the CC<sub>R</sub><sup>ADR1</sup> chimera with the first 50 amino acids of CC<sub>R</sub><sup>ADR1-L1</sup> (Figure S3C).

Canonical ubiquitination occurs on lysine residues. The first 50 amino acids of ADR1-L1 contain only two lysines, K34 and K48, that are conserved in ADR1-L2. The CC<sub>R</sub> domain from ADR1 instead features glutamate (E35) and arginine (R49) in these two positions (Figure S3B). The E35 and R49 residues may enable ADR1 to evade being targeted by AvrPtoB. To test this hypothesis, we mutated E35 and R49 of the CC<sub>R</sub><sup>ADR1</sup> to lysine (E35K and R49K) and examined the effects of the two mutations on AvrPtoB susceptibility. When both E35K and R49K were introduced, cell death triggered by CC<sub>R</sub><sup>ADR1</sup> was dramatically inhibited by AvrPtoB (Figures 3D and S3D). As expected, CC<sub>R</sub><sup>ADR1</sup> with E35K/R49K substitutions was ubiquitinated by AvrPtoB (Figure 3E). We also introduced these changes in the context of the full-length ADR1<sup>D461V</sup> gain-of-function variant, which became susceptible to suppression by AvrPtoB as well (Figures 3F and S3E). Conversely, when K34 and K48 of ADR1-L1<sup>D489V</sup> were mutated to glutamate and arginine, ADR1-L1<sup>D489V</sup>-triggered cell death could no longer be suppressed by AvrPtoB (Figures 3F and S3E). Taken together, our results indicate that the K34 and K48 residues are the functionally relevant sites in the CC<sub>R</sub> domain of ADR1-L1 that are ubiquitinated by AvrPtoB. Because ADR1 features different residues in these positions, E35 and R49, it evades suppression of its activity by AvrPtoB.

To understand the evolutionary history of changes at the CC<sub>R</sub> residues crucial for targeting by AvrPtoB, we reconstructed the

phylogeny of 552 ADR1 homologs from angiosperms. The 117 Brassicaceae homologs form a single clade, indicating that diversification occurred only in the Brassicaceae, with the ADR1 clade apparently being younger than the ADR-L1 clade (Figure S3F). Focusing on the two lysine residues targeted by AvrPtoB, we found that an ADR1 homolog from *Tarenaya hasleriana*, at the base of the Brassicales, encodes a lysine corresponding to position 48 in ADR1-L1, but not at position 34. In the Brassicaceae, the ADR-L1 and ADR-L2 homologs show similar profiles, with lysine being the most common residue at position 46/48, whereas lysine is found in that position only in a minority of ADR1 homologs. At position 32/34, several ADR1-L1/L2 homologs have a lysine, but lysine is never found at that position in ADR1 (Figure S3G). Notably, lysines at these two positions are exceedingly rare in ADR1 homologs outside of the Brassicaceae, suggesting an unknown trade-off that led to the evolution of lysines at these positions in the Brassicaceae, despite these residues being targets of AvrPtoB.

#### adr1-L1-null mutants express constitutive immunity

The *adr1-L1-1* mutant, reported to carry a transfer DNA (T-DNA) insertion disrupting the first exon of *ADR1-L1*, has been used to characterize the effects of *ADR1-L1* on plant immunity, with the conclusion that the mutant on its own has no major phenotypes,<sup>26,27</sup> although this allele enhances *snc1* gain-of-function autoimmune defects, as do two EMS-induced *ADR1-L1* alleles, *muse15-1* and *muse15-2*.<sup>27</sup> To determine whether *adr1-L1-1* is indeed a knockout allele, we used an amplicon that spans the first and second exon of *ADR1-L1* to quantify mRNA expression in RT-qPCR (real-time qPCR) assays. We found that the T-DNA

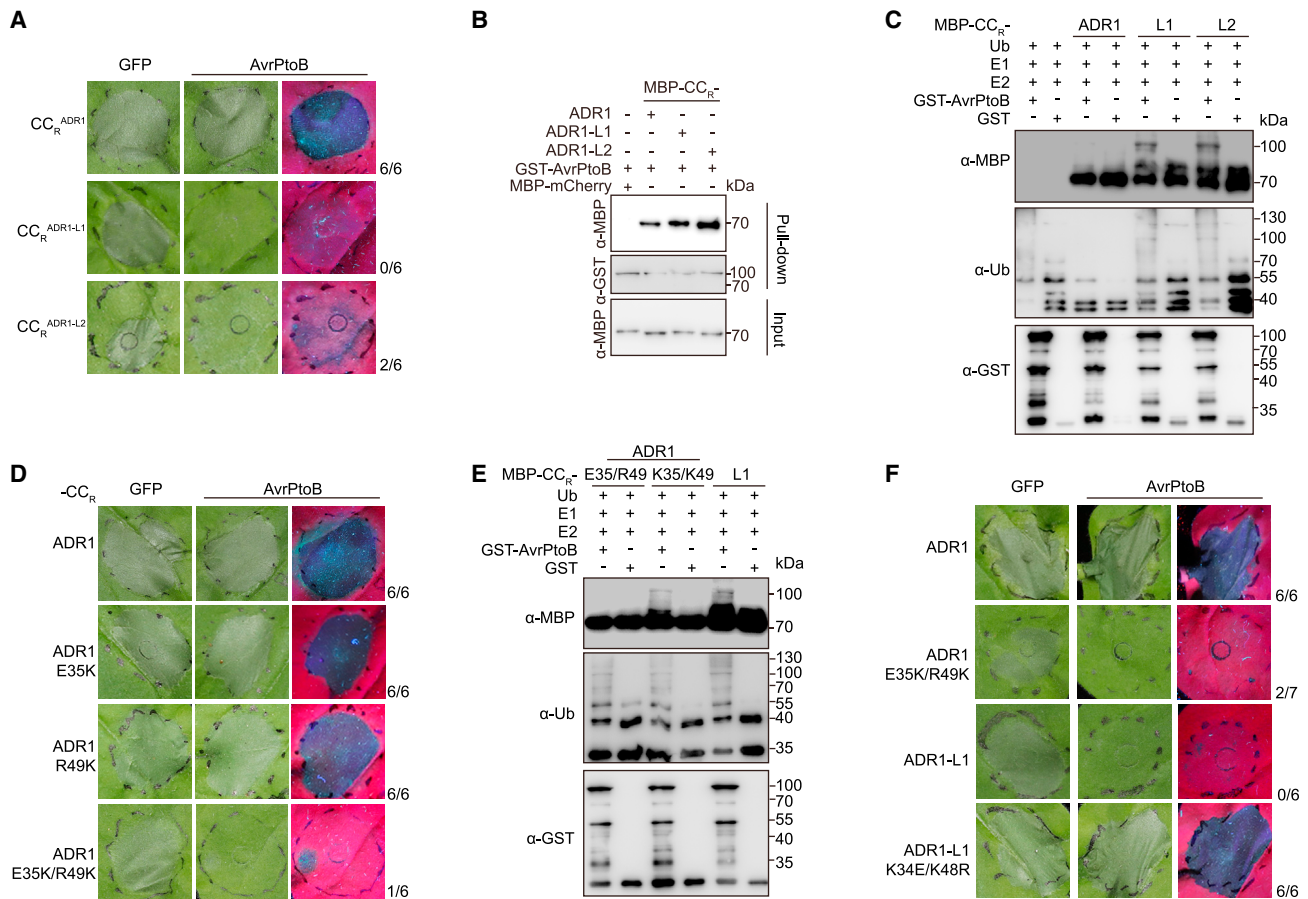


**Figure 3. Two lysines in the CC<sub>R</sub> domain are required for AvrPtoB-dependent suppression of ADR1-L1<sup>D489V</sup> activity**  
 (A) AvrPtoB fully and partially suppresses HR triggered by CC<sub>R</sub><sup>ADR1-L1</sup> and CC<sub>R</sub><sup>ADR1-L2</sup>, but not HR triggered by CC<sub>R</sub><sup>ADR1</sup> in *N. benthamiana*.  
 (B) AvrPtoB associates with the CC<sub>R</sub> domains of the three ADR1 homologs *in vitro*, as shown by pull-down assays with proteins purified from *E. coli*.  
 (C) AvrPtoB ubiquitinates CC<sub>R</sub><sup>ADR1-L1</sup> and CC<sub>R</sub><sup>ADR1-L2</sup>, but not CC<sub>R</sub><sup>ADR1</sup>, as shown *in vitro* with proteins purified from *E. coli*.  
 (D) AvrPtoB suppresses HR triggered by the E35K R49K mutant of ADR1 in *N. benthamiana*.  
 (E) AvrPtoB ubiquitinates mutant CC<sub>R</sub><sup>ADR1</sup> at E35K and R49K but not wild-type CC<sub>R</sub><sup>ADR1</sup>, as shown by *in vitro* ubiquitination with proteins purified from *E. coli*.  
 (F) AvrPtoB suppresses HR triggered by full-length ADR1<sup>D489V</sup> with E35K/R49K mutations in *N. benthamiana*. Conversely, AvrPtoB no longer suppresses HR triggered by ADR1-L1<sup>D489V</sup> upon introduction of the K34E/K48R mutations. Numbers on the right (A, D, and F) indicate leaves with HR over all infiltrated leaves tested. Experiments were performed three times, with similar results. See also Figure S3.

mutant still expressed about 30% of the wild-type amount of ADR1-L1 mRNA (Figures S4A and S4B), indicating that *adr1-L1-1* is only a knockdown allele.

We generated a null mutant of ADR1-L1, *adr1-L1-c1*, by deleting the full coding region of ADR1-L1 through CRISPR-Cas9 gene editing (Figure 4A). No ADR1-L1 expression was detected in the mutant by RT-qPCR (Figure S4C). Plants carrying this allele, *adr1-L1-c1*, were stunted and had curly leaves (Figure 4A), two hallmarks of autoimmunity in Arabidopsis.<sup>28</sup> To exclude the possibility that the phenotypes of *adr1-L1-c1* mutant were due to CRISPR-Cas9 off-target effects, we transformed ADR1-L1 driven by its native promoter into *adr1-L1-c1* mutants. Dwarfing and leaf curling were rescued in the complementation lines (Figure 4A), confirming that the observed phenotypes are due to knockout of ADR1-L1. Three additional independent CRISPR-Cas9 mutants (*adr1-L1-c2*, *adr1-L1-c3*, and *adr1-L1-c4*), which had either a small inversion or small deletions in the region en-

coding the CC<sub>R</sub> domain, were also stunted in size and had curly leaves, mimicking the *adr1-L1-c1* mutants (Figure 4A).

We next quantified expression of the defense marker gene *PR1* to determine whether the phenotypes of the new *adr1-L1* mutants were indeed due to autoimmunity. *PR1* expression was increased in all four new *adr1-L1* mutants (Figure 4B), and this increase was reversed in the *adr1-L1-c1* complementation lines. Growth of the bacterial pathogen *Pst* DC3000 was impaired in the four new *adr1-L1* mutants, and this mutant phenotype was again rescued in the *adr1-L1-c1* complementation lines (Figure 4C). To confirm that the absence of reported phenotypes for the T-DNA allele *adr1-L1-1*<sup>26,27</sup> did not result from differences in growth conditions, we grew it alongside the new *adr1-L1-c1* mutant, confirming that only the T-DNA knockdown allele appeared normal (Figure S4D). Collectively, these results demonstrate that a complete knockout of ADR1-L1 leads to spontaneous activation of immunity.

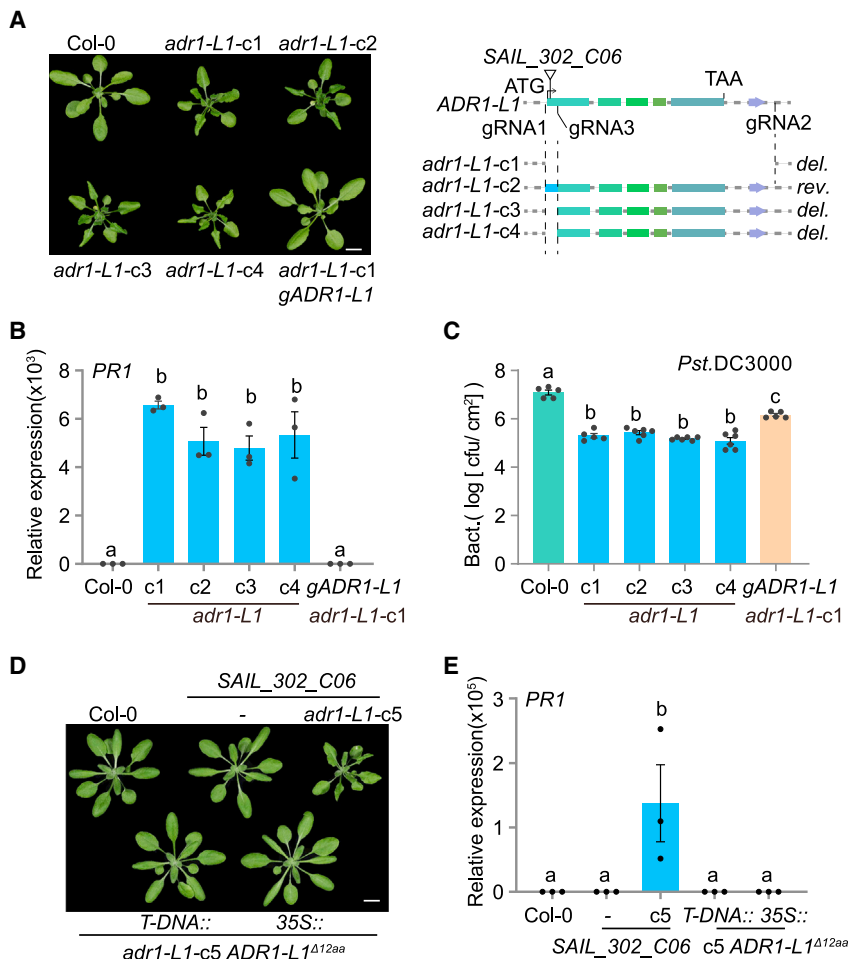


**Figure 4. Inactivation of *ADR1-L1* causes autoimmunity**

(A) Left, four independent *adr1-L1*-null mutants generated by CRISPR-Cas9 have typical autoimmune phenotypes, which are rescued by a genomic *ADR1-L1* copy (“*gADR1-L1*”). Right: diagram of T-DNA insertion in *adr1-L1-1*, the region targeted by guideRNAs (gRNAs) for CRISPR-Cas9-mediated inactivation, and the resultant *adr1-L1* null alleles. Scale bars: 10 mm.

(B) *PR1* expression in plants in (A) was quantified by RT-qPCR, showing increased *PR1* expression in *adr1-L1* mutants.

(C) *adr1-L1* mutants are more resistant to *Pst* DC3000 infection. Growth of *Pst* DC3000 in indicated Arabidopsis lines at 3 days post-infiltration (dpi) infected via syringe infiltration ( $OD_{600} = 0.002$ ). (D) The T-DNA mutant line SAIL\_302\_C06 is a partial loss-of-function allele of *ADR1-L1*. 4-week-old plants are shown. Scale bars: 10 mm.

(E) *PR1* expression in plants in (D) was quantified by RT-qPCR, showing increased *PR1* expression also in the *adr1-L1-c5* mutant generated in the *adr1-L1-1* background. Data in (B), (C), and (E) represent the mean and standard error ( $n = 3, 5, \text{ and } 3$  biologically independent samples for (B), (C), and (E), respectively).  $p < 0.05$ , one-way ANOVA followed by Tukey’s post hoc test, letters indicate significantly different groups. See also Figure S4.

Further analysis of the *adr1-L1-1* T-DNA mutant showed that this allele produces a 5’ truncated transcript, with the T-DNA fragment providing a new start codon that should produce a nearly full-length protein lacking only amino acids 2 to 13 (ADR1-L1 <sup>$\Delta$ 12aa</sup>) (Figures S4B–S4F). Deletion of *ADR1-L1* including the inserted T-DNA using CRISPR-Cas9 in the *adr1-L1-1* background led to dwarfism and increased *PR1* expression, which was reversed when the plants were transformed with a construct containing *ADR1-L1* <sup>$\Delta$ 12aa</sup> driven by the 3’ region of the T-DNA or the CaMV35S promoter (Figures 4D and 4E). These results confirm that *adr1-L1-1* is only a partial loss-of-function allele that does not cause overt autoimmunity.

#### ***adr1-L1*-null mutant defects are *SNC1* dependent**

The defense marker *PR1*, which is greatly increased in *adr1-L1* null mutants, is regulated by SA, and SA signaling in turn is protected by *EDS1* and *PAD4*.<sup>29</sup> To begin to uncover the mechanism underlying the spontaneous activation of immunity in *adr1-L1* null mutants, we first crossed *adr1-L1-c1* mutants to plants deficient for the salicylic acid biosynthesis gene *SID2* (SALICYLIC ACID INDUCTION DEFICIENT 2) or for *PAD4* and *EDS1*. The morphological defects of *adr1-L1-c1* were partially suppressed by *sid2-2* and fully suppressed by *eds1-2* and *pad4-1* (Figure S5A).

Because autoimmunity often results from inappropriate activation of NLR activity, we speculated that the autoimmune phenotype of *adr1-L1* mutants might result from genetic interaction with other NLRs. To identify such NLR candidates, we exploited the extensive variation in NLR complements in different Arabidopsis accessions,<sup>30</sup> and deleted *ADR1-L1* in the Arabidopsis accessions Est-1, C24, and Ws-2. Different from Col-0 and C24, inactivation of *ADR1-L1* in Ws-2 and Est-1 did not cause obvious morphological defects (Figure 5A). An F<sub>2</sub> mapping population was generated by crossing *adr1-L1* (Ws-2) and *adr1-L1-c1* (Col-0). Genetic linkage analysis identified a single large-effect locus on chromosome 4 that suppressed *adr1-L1* autoimmune defects. Fine mapping narrowed the interval to a ~130 kb region from 9.47 to 9.60 Mb on chromosome 4 (Figure S5B), which encompasses the *RPP4* cluster of *TNL* genes.

The *RPP4* cluster includes the extensively studied *TNL* gene *SNC1*, which is functional in Col-0, but not in Ws-2,<sup>31</sup> one of the two accessions in which the *adr1-L1* knockout phenotype is suppressed. To test whether *SNC1* is a natural modifier of *adr1-L1*, we transformed the *SNC1* (Col-0) genomic fragment into the *adr1-L1* (Ws-2) mutant. The transgenic plants resembled the *adr1-L1-c1* mutant of the Col-0 accession (Figure 5A). Furthermore, in Col-0, the *snc1-11* knockout allele suppressed morphological and molecular defects of *adr1-L1-c1* mutants (Figures 5B, S5C, and S5D), confirming that *SNC1* is a natural modifier of *ADR1-L1*. Dwarfism of the *adr1-L1-c1 snc1-11* double mutant was restored by introducing a wild-type *SNC1* genomic fragment, but not a fragment with the P-loop mutation

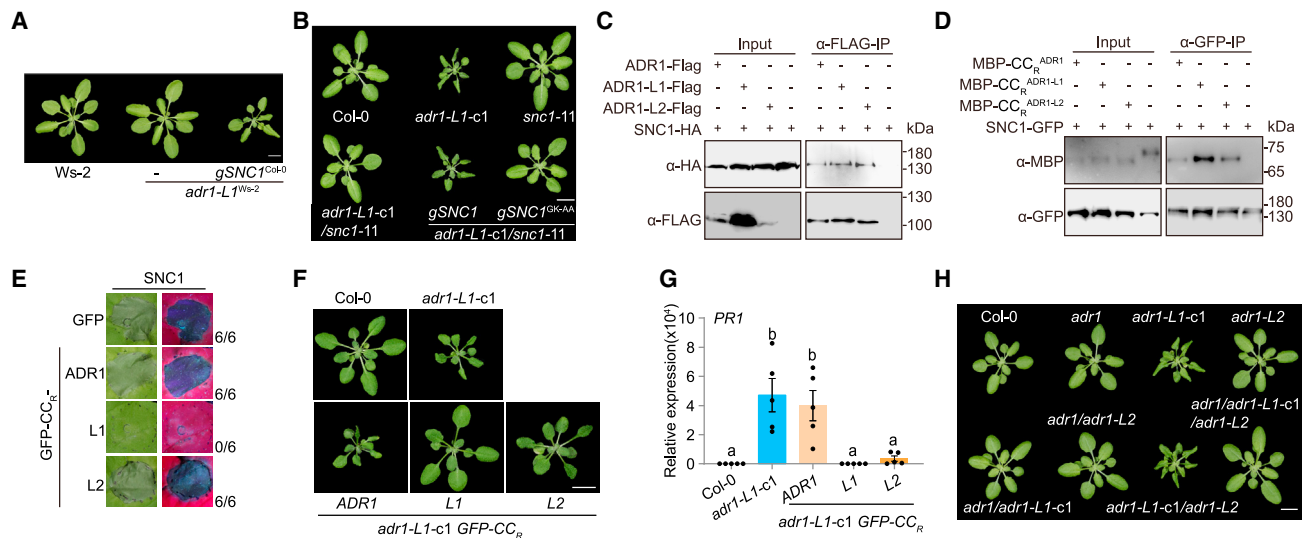


**Figure 5. SNC1 guards ADR1-L1 and ADR1-L2 and signals through ADR1**

(A) The natural loss-of-function *SNC1* allele in Ws-2 suppresses growth defects of *adr1-L1* null mutants in Ws-2. 4-week-old plants of Ws-2, *adr1-L1* (Ws-2), and *adr1-L1* (Ws-2) complemented with a *SNC1* genomic fragment from Col-0. Scale bars: 10 mm.

(B) The loss-of-function *snc1-11* allele suppresses growth defects of the *adr1-L1-c1* null mutant in Col-0. This effect is reversed by introduction of a wild-type *SNC1* genomic fragment, but not of the mutant *SNC1*<sup>GK-AA</sup> variant. Scale bars: 10 mm.

(C) SNC1 associates with the three ADR1 homologs, as shown by coIP assays in *N. benthamiana*.

(D) SNC1 interacts with the CC<sub>R</sub> domains of the three ADR1 homologs, as shown by semi-*in vitro* pull-down assays. SNC1-GFP and MBP-CC<sub>R</sub> proteins were purified from *N. benthamiana* and *E. coli*, respectively.

(E) The CC<sub>R</sub> domain of GFP-tagged ADR1-L1 suppresses SNC1-triggered HR in *N. benthamiana*. Numbers on the right indicate leaves with HR over all infiltrated leaves tested.

(F) Expression of GFP-tagged CC<sub>R</sub> domains of ADR1-L1 and ADR1-L2 but not ADR1 suppress the growth defects of *adr1-L1-c1*. Representative 4-week-old Arabidopsis T<sub>1</sub> transgenic plants with *p35S::GFP-CC<sub>R</sub><sup>ADR1</sup>*, *p35S::GFP-CC<sub>R</sub><sup>ADR1-L1</sup>* and *p35S::GFP-CC<sub>R</sub><sup>ADR1-L2</sup>* in *adr1-L1-c1*, grown in 23°C. Scale bars, 10 mm.

(G) *PR1* expression of 3-week-old T<sub>1</sub> transformants shown in (F). Data represent the mean and standard error of five independent T<sub>1</sub> transformants (n = 5 biologically independent samples, p < 0.05, one-way ANOVA followed by Tukey's post hoc test; letters indicate significantly different groups).

(H) 3-week-old *adr1-L1-c1* single and multiple mutants, grown at 23°C. Scale bars, 10 mm. Experiments in (C)–(E) were performed three times, with similar results. See also Figure S5.

*SNC1*<sup>GK-AA</sup> (Figure 5B). Together, these results show that *adr1-L1* mutant defects are mediated by *SNC1*, most likely through activation of *SNC1* signaling.

### SNC1 guards ADR1-L1/L2 and signals through ADR1

The genetic interaction of *SNC1* and *ADR1-L1* prompted us to test their physical interaction. *SNC1* was pulled down by all three ADR1 homologs in coIP assays in *N. benthamiana* (Figure 5C). *In vitro* pull-down experiments pointed to *SNC1* interacting, likely with different affinities, with the CC<sub>R</sub> domains of the three ADR1 homologs (Figure 5D).

Given the genetic and physical interaction between ADR1-L1 and *SNC1*, we hypothesized that *SNC1*, a sensor NLR, may guard ADR1-L1 through binding its CC<sub>R</sub> domain, with loss of ADR1-L1 leading to *SNC1* activation, as seen with some other NLRs that directly guard cellular targets.<sup>17</sup> Although the CC<sub>R</sub> of ADR1-L1 could trigger cell death in *N. benthamiana*, the N-terminal GFP-tagged CC<sub>R</sub> is inactive, likely due to inhibition of channel activity (Figures S5E and S5F). We thus took advantage of this inactive form of GFP-CC<sub>R</sub> to test whether *SNC1* was guarded by the CC<sub>R</sub> of ADR1-L1. Transient expression of *SNC1* on its own triggered cell death in *N. benthamiana*, which could be suppressed by co-expression of GFP-CC<sub>R</sub><sup>ADR1-L1</sup>, but not GFP-

CC<sub>R</sub><sup>ADR1</sup> or GFP-CC<sub>R</sub><sup>ADR1-L2</sup> (Figures 5E, S5E, and S5F). In Arabidopsis, overexpression of GFP-CC<sub>R</sub><sup>ADR1-L1</sup> completely suppressed the phenotypes of *adr1-L1-c1* mutants (T<sub>1</sub> mutants, n = 26). Overexpression of GFP-CC<sub>R</sub><sup>ADR1-L2</sup> could sometimes partially suppress *adr1-L1-c1* phenotypes (7/28 T<sub>1</sub> plants), whereas GFP-CC<sub>R</sub><sup>ADR1</sup> was ineffective (n = 56) (Figures 5F and 5G). We conclude that through monitoring CC<sub>R</sub> domains, *SNC1* mainly guards ADR1-L1 and, to a lesser extent, ADR1-L2, but not ADR1. A minor role of *SNC1* in guarding ADR1-L2 was further supported by the observation that the *adr1-L2* T-DNA (*SALK\_126422*) mutation slightly but significantly enhanced the *adr1-L1-c1* phenotype (Figures 5H and S5H). Unlike the *adr1-L1* mutants, which are dwarfed, both the *adr1-L2* T-DNA and CRISPR-Cas9 alleles resembled wild-type plants (Figure S5I). This suggests that the minor effects of the *adr1-L2* T-DNA mutation are not due to a partial loss of function. The more prominent role of ADR1-L1 in serving as a guard of *SNC1* is likely due to its higher expression than ADR1-L2 (Figure S5J), which allows ADR1-L1 to sequester and suppress the activity of more *SNC1* protein molecules.

Phenotypic abnormalities in the *adr1-L1-c1* single and the *adr1-L1-c1 adr1-L2* double mutants were completely suppressed in the presence of the *adr1* mutation (Figure 5H).

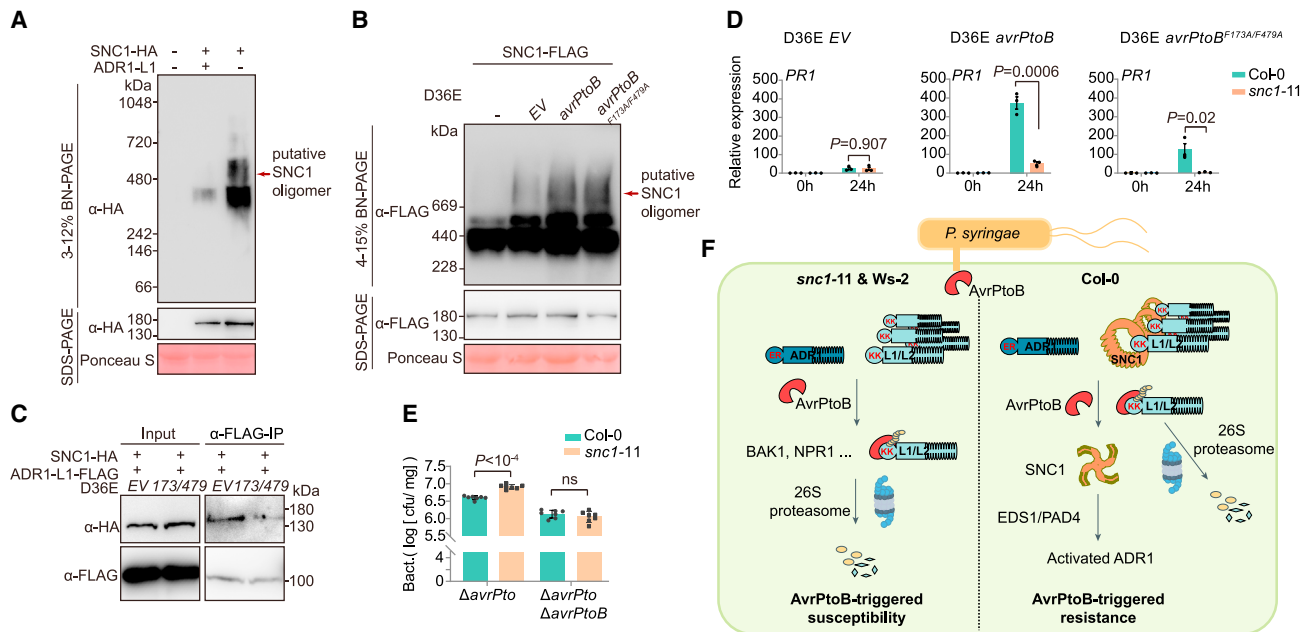


**Figure 6. AvrPtoB induces oligomerization of SNC1 and activates SNC1-dependent immune responses**

(A) Absence of ADR1-L1 stimulates SNC1 oligomerization in Arabidopsis, as shown by BN-PAGE and SDS-PAGE. Arrow points to apparent higher-order SNC1 complexes, likely SNC1 tetramers.  
 (B) AvrPtoB enhances SNC1 oligomerization as shown by BN-PAGE and SDS-PAGE. Arrow points to potential SNC1 complexes.  
 (C) The E3 ligase dead variant AvrPtoB<sup>F173A/F479A</sup> interferes with the interaction between ADR1-L1 and SNC1, as shown by coIP assays in transgenic Arabidopsis.  
 (D) *PR1* expression of Col-0 and *snc1-11* after flood inoculation with *Pst* DC3000 D36E carrying empty vector, *AvrPtoB*, or *AvrPtoB*<sup>F173A/F479A</sup> (OD<sub>600</sub> = 0.3), as measured by RT-qPCR. Data represent the mean and standard error of three biological replicates (n = 3 biologically independent samples, p values from Student's t test).  
 (E) AvrPtoB activates SNC1-dependent resistance to *Pst* DC3000. Bacterial growth assays of *Pst* DC3000, *Pst* DC3000 Δ*avrPto*, and *Pst* DC3000 Δ*avrPto* Δ*avrPtoB* on Col-0 and *snc1-11* at 2 dpi after flood inoculation (OD<sub>600</sub> = 0.02, n = 7 biologically independent samples, p values from Student's t test). Experiments in (A)–(E) were performed three times, with similar results.  
 (F) Working model. In absence of functional SNC1, as in *Ws-2* and *snc1-11*, AvrPtoB ubiquitinates ADR1-L1, and, to a lesser extent, ADR1-L2, to promote their degradation, preventing activation of immunity. In the presence of SNC1, degradation of ADR1-L1 and ADR1-L2 induced by AvrPtoB activates oligomerization of the SNC1 guard, which relays signals through ADR1 to trigger downstream immune responses. See also Figure S6.

The reliance of SNC1-mediated autoimmunity on ADR1 is consistent with the fact that PAD4, which forms complexes with ADR1 homologs,<sup>11</sup> is indispensable for SNC1 signaling.<sup>32</sup> Taken together, these results indicate that ADR1-L1 and ADR1-L2 are guarders of SNC1, which in turn signals via ADR1 to activate downstream responses.

### SNC1 recognizes AvrPtoB through ADR1-L1

Structural studies have revealed how oligomerization of TNL proteins, ROQ1 and RPP1, and CNL proteins, ZAR1 and Sr35, is associated with their activation.<sup>9,33–36</sup> We therefore used BN (blue native)-PAGE to compare the behavior of 3xHA-tagged SNC1 in *snc1-11* and *adr1-L1-c1 snc1-11* plants. As shown in Figure 6A, in the absence of ADR1-L1, SNC1 protein shifts to a slow-migrating species of 480–720 kDa, which likely corresponds to SNC1 tetramers. This shift is also observed in *adr1 adr1-L1 adr1-L2* triple mutants, but not in *adr1* mutants (Figure S6A). We conclude that the loss of ADR1-L1 is sufficient to trigger oligomerization of SNC1, with the SNC1 oligomer constituting the active form.

Since ubiquitination of ADR1-L1 by AvrPtoB leads to the loss of ADR1-L1, akin to the situation in *adr1-L1-c1* mutants, we also

examined whether AvrPtoB induced SNC1 oligomerization. As shown in Figure 6B, infiltration of *Pst* DC3000 D36E expressing *AvrPtoB* induced a slow-migrating SNC1 species of 480–720 kDa, similar to what had been observed in *adr1-L1-c1* mutants (Figure 6A), confirming that SNC1 acts as a guard for the AvrPtoB target ADR1-L1. Unexpectedly, infiltration of *Pst* DC3000 D36E carrying the E3 ligase-dead *AvrPtoB*<sup>F173A/F479A</sup> had a similar effect on SNC1. Since both SNC1 and AvrPtoB interact with the CC<sub>R</sub> domain of ADR1-L1, AvrPtoB<sup>F173A/F479A</sup> might compete with SNC1 for interaction with ADR1-L1, which could result in the failure of ADR1-L1 to prevent oligomerization of SNC1. To test this hypothesis, we co-expressed ADR1-L1-GFP and SNC1-HA with AvrPtoB<sup>F173A/F479A</sup>-FLAG for coIP assays in *N. benthamiana*. In support of the proposed scenario, AvrPtoB<sup>F173A/F479A</sup> substantially reduced the ability of ADR1-L1 to pull down SNC1, which was further confirmed by coIP assays with bacteria-infected ADR1-L1-FLAG and SNC1-HA co-expressing transgenic plants (Figures 6C and S6B).

Overexpression of AvrPtoB induces dramatic autoimmunity in the Col-0 accession,<sup>37</sup> which we hypothesized could be due to loss of ADR1-L1 and concomitant activation of SNC1. Attempts to generate 35S::AvrPtoB-FLAG transgenic lines, which we

could have used for epistasis tests with *snc1* loss-of-function mutants, were not successful, likely due to extreme autoimmunity. As an alternative, we measured expression of the defense marker *PR1* in Arabidopsis upon delivery of *AvrPtoB* or *AvrPtoB*<sup>F173A/F479A</sup> by DC3000 D36E. As shown in Figure 6D, *snc1-11* mutants expressed significantly less *PR1* than wild-type plants in these trials. Moreover, the increased growth of *Pst* DC3000  $\Delta$ *avrPto* in *snc1-11* was dependent on *AvrPtoB*, since no difference was seen between *snc1-11* and wild-type plants infiltrated with *Pst* DC3000  $\Delta$ *avrPto*  $\Delta$ *avrPtoB* (Figure 6E). *Pst* DC3000  $\Delta$ *avrPto*  $\Delta$ *avrPtoB* complemented with *avrPtoB*<sup>F173A/F479</sup> grew to similar levels in wild-type and *snc1-11* plants (Figure S6C), likely due to modest activation of immune responses triggered by *AvrPtoB*<sup>F173A/F479</sup>. We conclude that the degradation of ADR1-L1 initiated by *AvrPtoB* activates immune responses mediated by SNC1.

## DISCUSSION

The conserved helper NLR proteins of the ADR1 family are key ETI components.<sup>17</sup> We found that the bacterial effector *AvrPtoB* targets two ADR1 homologs, *ADR1-L1* and *ADR1-L2*, and that these are in turn guarded by the sensor NLR SNC1. Our findings demonstrate a concept in the co-evolution between pathogen effectors and plant immune receptors, and they reveal also at least one of the long-sought-after functions of SNC1 in plant immunity.

Paradoxically, SNC1 activates defense upon detecting *AvrPtoB*'s action on ADR1-L1 and ADR1-L2; however, *Pst* DC3000 can still cause disease in Arabidopsis plants with functional SNC1. Although *Pst* DC3000 has been reported to grow to similar levels on Col-0 and Col-0 *snc1-11* mutants when inoculated at an approximate OD<sub>600</sub> (Optical Density at 600 nm) = 0.0001 (10<sup>6</sup> colony-forming unit [CFU]/mL),<sup>31</sup> we found *Pst* DC3000  $\Delta$ *avrPto* grows to higher levels on *snc1-11* than wild-type plants when inoculated at OD<sub>600</sub> = 0.02 (Figure 6E). Moreover, infiltration of Arabidopsis leaves with *Pst* DC3000 D36E *avrPtoB* at OD<sub>600</sub> = 0.3 triggers SNC1 oligomerization (Figure 6B) and elevates *PR1* expression; both of these outcomes are compromised in *snc1-11* mutants (Figure 6D). The recognition of *AvrPtoB* by SNC1 is further supported by the severe autoimmunity observed in Arabidopsis Col-0 upon *AvrPtoB* overexpression.<sup>37</sup> We interpret our results as being consistent with the quantitative nature of the combined output of PTI and ETI, which is weakened by effector-triggered susceptibility (ETS) resulting from the action of 36 *Pst* DC3000 effectors. If the potentiation of PTI by ETI<sup>4,5</sup> is sufficiently weakened by ETS, plants are unable to restrict *Pst* DC3000 growth. Whether a particular plant/microbe interaction results in disease or susceptibility depends upon the balance between the stimulation of PTI and ETI pathways, and the effectiveness of PTI and ETI attenuation by pathogen effectors. Importantly, whereas ETI usually results in a level of immunity that confers resistance to pathogen infection, weak activation of ETI may not completely preclude susceptibility.

*AvrPtoB* is a conserved effector found in the genomes of diverse Gram-negative bacteria, including *Pseudomonas*, *Xanthomonas*, and *Erwinia*.<sup>38</sup> *AvrPtoB* has been shown to target and ubiquitinate a wide range of proteins, including several pattern-recognition receptors and PTI key component BAK1 (BRASSINOSTEROID RECEPTOR-ASSOCIATED KINASE 1),<sup>39</sup>

the master regulator of salicylic acid signaling, NPR1 (NON-EXRESSER OF PR GENES 1),<sup>40</sup> and an exocyst subunit.<sup>37</sup> Here, we show that *AvrPtoB* can dampen both PTI and ETI, by identifying the central ETI components ADR1-L1 and ADR1-L2 as *AvrPtoB* targets.

Pathogen effectors have two roles: one is to manipulate host physiology for the colonizer's benefit and the other—and the one most recent work has focused on—is to suppress host defenses, especially those related to PTI.<sup>41</sup> Examples of effectors targeting NLRs come from the *P. infestans* effector AVRcap1b and the cyst nematode effector SS15, which suppress the Solanaceae-specific helper NLRs NRC2 and NRC3, either by affecting their negative regulator NtTOL9a or by preventing their oligomerization and activation.<sup>22,23</sup> We add to these insights, by revealing not only that helper NLRs ADR1-L1 and ADR1-L2 are targeted by *P. syringae* effector *AvrPtoB* but also that *AvrPtoB*-induced degradation of ADR1-L1 and ADR1-L2 is monitored by the sensor NLR SNC1 (Figure 6F). Pathogen effectors of independent origin often converge on conserved targets with essential roles in plant immunity.<sup>42</sup> ADR1 homologs, which are widespread in the plant kingdom,<sup>7</sup> clearly fulfill this definition, and it is therefore not unlikely that other effectors targeting ADR1 homologs await discovery. Similarly, it will be of interest to learn whether ADR1 homologs in other species are guarded by other NLRs, since SNC1 is an Arabidopsis-specific NLR.

One of the reasons that there is a rich literature on SNC1 is that its knockout suppresses, albeit to different degrees, autoimmunity resulting from changes in a wide range of proteins.<sup>17</sup> Given the role of SNC1 as a guard of ADR1 homologs, the genes that interact with SNC1 mutant alleles might encode negative regulators of SNC1, potentially by affecting the interaction between SNC1 and ADR1 homologs. Guarding of ADR1 homologs might, however, not be the only role of SNC1, which has been proposed to be a more general amplifier of ETI.<sup>43</sup> SNC1 was found to enhance *avrRpt2*- and *avrRps4*-induced resistance,<sup>43</sup> which depends on ADR1 homologs.<sup>44</sup> We propose that the formation of ADR1 oligomers triggered by interaction of effectors such as *AvrRpt2* and *AvrRps4* with their cognate NLR immune receptors could displace SNC1 from the ADR1-L1/L2-SNC1 guardee-guard complex, which in turn might amplify downstream immune responses via ADR1. Regardless of any other roles, however, SNC1 clearly fits the definition of a resistance protein for indirect recognition of the bacterial effector *AvrPtoB*. The importance of being able to detect *AvrPtoB* is also apparent from the fact that, as with other effectors,<sup>17</sup> *AvrPtoB* can be recognized by other NLRs, including tomato Prf via its guardee Pto, which directly interacts with *AvrPtoB*.<sup>45,46</sup>

In summary, we have demonstrated that bacterial *AvrPtoB* ubiquitinates conserved key components of ETI, which in turn is detected by the plant host through the sensor NLR SNC1. Our work highlights how the same pathway can be a target of pathogen effector proteins and at the same time be used to protect the host from these effectors. In addition, we demonstrate how sequence diversification enables a partially redundant helper NLR to evade effector suppression and thereby preserve the integrity of ETI.

## Limitations of the study

Which fraction of ADR1 homologs is targeted for degradation after ubiquitination by *AvrPtoB* during infection is still unclear. Our

lab-based infection assays cannot fully capture the degree of immunity activated by AvrPtoB during natural bacterial infections, which are thought to start often with very small inocula. In addition, future studies are needed to elucidate why ADR1-L1 and ADR1-L2, but not ADR, are guarded by SNC1, although all three ADR1 homologs can interact with SNC1.

## STAR★METHODS

Detailed methods are provided in the online version of this paper and include the following:

- **KEY RESOURCES TABLE**
- **RESOURCE AVAILABILITY**
  - Lead contact
  - Materials availability
  - Data and code availability
- **EXPERIMENTAL MODEL AND SUBJECT DETAILS**
  - Arabidopsis
  - *Nicotiana benthamiana*
  - Bacterial Strains
- **METHOD DETAILS**
  - Cell death assays
  - Generation of transgene-free gene-edited lines
  - Generation of high-order mutants
  - RT-qPCR
  - Phylogeny analysis
  - Constructs and transgenic lines
  - TurboID based biotinylation in Arabidopsis seedling
  - Map-based cloning
  - Bacterial infection
  - AvrPtoB-induced protein degradation in Arabidopsis
  - Split-luciferase complementation assay
  - Co-immunoprecipitation
  - In vitro ubiquitination assays
  - In vitro pull-down assays
  - Blue Native-PAGE
- **QUANTIFICATION AND STATISTICAL ANALYSIS**

## SUPPLEMENTAL INFORMATION

Supplemental information can be found online at <https://doi.org/10.1016/j.chom.2023.10.006>.

## ACKNOWLEDGMENTS

We thank Lei Li (CAS), Guozhi Bi (CAU), and Yule Liu (THU) for the discussion. We thank Wenbo Ma (TSL) and Robert Heal (TSL) for critical reading of the manuscript. We thank Lei Li and He Zhao (TSL) for technical support with the BN-PAGE experiment. We thank Xin Li (UBC) for helper NLR mutant seeds, Hailei Wei (CAAS) for the *Pst* DC3000 D36E strain, Jun Liu (CAU) for the *Pst* DC3000 T3SS effector vector library. R.W. was supported by the EU Horizon 2020 research and innovation program under the Marie Skłodowska-Curie scheme (H2020-MSCA-IF-2014-655295). J.D.G.J. was supported by the Gatsby Foundation (UK). D.W. was supported by ERC-SyG PATHOCOM 951444 and the Max Planck Society. J.-H.H. was supported by the EUs Horizon 2020 research and innovation program under the Marie Skłodowska-Curie scheme (no 897584). W.-S.Z. was supported by the National Key Research and Development Program, Ministry of Science and Technology of China (no 2022YFD1201802), the Ministry of Education of China (the 111 Project B13006), and the 2115 Talent Development Program of China Agricultural University (no 2020RC013).

## AUTHOR CONTRIBUTIONS

Conceptualization: J.-H.H. and W.-S.Z.; methodology: M.-Y.W., J.-B.C., R.W., H.-L.G., J.-H.H., and W.-S.Z.; formal analysis: M.-Y.W., J.-B.C., R.W., and W.-S.Z.; investigation: M.-Y.W., J.-B.C., R.W., H.-L.G., Y.C., Z.-J.L., L.-Y.W., C.L., S.-F.H., and M.-D.D.; writing – original draft: M.-Y.W., J.-B.C., J.-H.H., and W.-S.Z.; writing – review, and editing: H.-L.G., W.-S.Z., J.D.G.J., and D.W.; supervision: Y.-L.P., D.W., J.D.G.J., and W.-S.Z.; project administration: W.-S.Z.; funding acquisition: R.W., J.D.G.J., D.W., J.-H.H., and W.-S.Z.

## DECLARATION OF INTERESTS

D.W. holds equity in Computomics, which advises plant breeders. D.W. consults for KWS SE, a plant breeder and seed producer with activities throughout the world.

## INCLUSION AND DIVERSITY

We support inclusive, diverse, and equitable conduct of research.

Received: May 2, 2023

Revised: September 1, 2023

Accepted: October 6, 2023

Published: November 8, 2023

## REFERENCES

1. Jones, J.D.G., and Dangl, J.L. (2006). The plant immune system. *Nature* 444, 323–329.
2. Zhou, J.M., and Zhang, Y. (2020). Plant immunity: danger perception and signaling. *Cell* 181, 978–989.
3. Pruitt, R.N., Locci, F., Wanke, F., Zhang, L., Saile, S.C., Joe, A., Karelina, D., Hua, C., Fröhlich, K., Wan, W.-L., et al. (2021). The EDS1–PAD4–ADR1 node mediates Arabidopsis pattern-triggered immunity. *Nature* 598, 495–499.
4. Yuan, M., Jiang, Z., Bi, G., Nomura, K., Liu, M., Wang, Y., Cai, B., Zhou, J.M., He, S.Y., and Xin, X.F. (2021). Pattern-recognition receptors are required for NLR-mediated plant immunity. *Nature* 592, 105–109.
5. Ngou, B.P.M., Ahn, H.K., Ding, P., and Jones, J.D.G. (2021). Mutual potentiation of plant immunity by cell-surface and intracellular receptors. *Nature* 592, 110–115.
6. Tian, H., Wu, Z., Chen, S., Ao, K., Huang, W., Yaghmaiean, H., Sun, T., Xu, F., Zhang, Y., Wang, S., et al. (2021). Activation of TIR signalling boosts pattern-triggered immunity. *Nature* 598, 500–503.
7. Liu, Y., Zeng, Z., Zhang, Y.M., Li, Q., Jiang, X.M., Jiang, Z., Tang, J.H., Chen, D., Wang, Q., Chen, J.Q., et al. (2021). An angiosperm NLR Atlas reveals that NLR gene reduction is associated with ecological specialization and signal transduction component deletion. *Mol. Plant* 14, 2015–2031.
8. Bi, G., Su, M., Li, N., Liang, Y., Dang, S., Xu, J., Hu, M., Wang, J., Zou, M., Deng, Y., et al. (2021). The ZAR1 resistosome is a calcium-permeable channel triggering plant immune signaling. *Cell* 184, 3528–3541.e12.
9. Förderer, A., Li, E., Lawson, A.W., Deng, Y.N., Sun, Y., Logemann, E., Zhang, X., Wen, J., Han, Z., Chang, J., et al. (2022). A wheat resistosome defines common principles of immune receptor channels. *Nature* 610, 532–539.
10. Jacob, P., Kim, N.H., Wu, F., El-Kasmi, F., Chi, Y., Walton, W.G., Furzer, O.J., Lietzan, A.D., Sunil, S., Kempthorn, K., et al. (2021). Plant “helper” immune receptors are Ca<sup>2+</sup>-permeable nonselective cation channels. *Science* 373, 420–425.
11. Huang, S., Jia, A., Song, W., Hessler, G., Meng, Y., Sun, Y., Xu, L., Laessle, H., Jirschtzka, J., Ma, S., et al. (2022). Identification and receptor mechanism of TIR-catalyzed small molecules in plant immunity. *Science* 377, eabq3297.

12. Wu, Z., Li, M., Dong, O.X., Xia, S., Liang, W., Bao, Y., Wasteneys, G., and Li, X. (2019). Differential regulation of TNL-mediated immune signaling by redundant helper CNLs. *New Phytol.* **222**, 938–953.
13. Castel, B., Ngou, P.M., Cevik, V., Redkar, A., Kim, D.S., Yang, Y., Ding, P., and Jones, J.D.G. (2019). Diverse NLR immune receptors activate defence via the RPW8-NLR NRG1. *New Phytol.* **222**, 966–980.
14. Zhang, Y., Goritschnig, S., Dong, X., and Li, X. (2003). A gain-of-function mutation in a plant disease resistance gene leads to constitutive activation of downstream signal transduction pathways in suppressor of npr1-1, constitutive 1. *Plant Cell* **15**, 2636–2646.
15. Stokes, T.L., Kunkel, B.N., and Richards, E.J. (2002). Epigenetic variation in Arabidopsis disease resistance. *Genes Dev.* **16**, 171–182.
16. Li, X., Clarke, J.D., Zhang, Y., and Dong, X. (2001). Activation of an EDS1-mediated R-gene pathway in the snc1 mutant leads to constitutive, NPR1-independent pathogen resistance. *Mol. Plant Microbe Interact.* **14**, 1131–1139.
17. van Wersch, S., Tian, L., Hoy, R., and Li, X. (2020). Plant NLRs: the whistleblowers of plant immunity. *Plant Commun.* **1**, 100016.
18. Zhu, W., Zaidem, M., Van de Weyer, A.L., Gutaker, R.M., Chae, E., Kim, S.T., Bemm, F., Li, L., Todesco, M., Schwab, R., et al. (2018). Modulation of ACD6 dependent hyperimmunity by natural alleles of an Arabidopsis thaliana NLR resistance gene. *PLoS Genet.* **14**, e1007628.
19. Wei, H.L., Chakravarthy, S., Mathieu, J., Helmann, T.C., Stodghill, P., Swingle, B., Martin, G.B., and Collmer, A. (2015). Pseudomonas syringae pv. tomato DC3000 type III secretion effector polymutants reveal an interplay between HopAD1 and AvrPtoB. *Cell Host Microbe* **17**, 752–762.
20. Martel, A., Laflamme, B., Breit-McNally, C., Wang, P., Lonjon, F., Desveaux, D., and Guttman, D.S. (2022). Metaeffector interactions modulate the type III effector-triggered immunity load of Pseudomonas syringae. *PLoS Pathog.* **18**, e1010541.
21. Wei, H.L., Zhang, W., and Collmer, A. (2018). Modular study of the type III effector repertoire in Pseudomonas syringae pv. tomato DC3000 reveals a matrix of effector interplay in pathogenesis. *Cell Rep.* **23**, 1630–1638.
22. Derevnina, L., Contreras, M.P., Adachi, H., Upson, J., Vergara Cruces, A., Xie, R., Sktenar, J., Menke, F.L.H., Mugford, S.T., MacLean, D., et al. (2021). Plant pathogens convergently evolved to counteract redundant nodes of an NLR immune receptor network. *PLoS Biol.* **19**, e3001136.
23. Contreras, M.P., Pai, H., Selvaraj, M., Toghiani, A., Lawson, D.M., Tumtas, Y., Duggan, C., Yuen, E.L.H., Stevenson, C.E.M., Harant, A., et al. (2023). Resurrection of plant disease resistance proteins via helper NLR bioengineering. *Sci. Adv.* **9**, eadg3861.
24. Janjusevic, R., Abramovitch, R.B., Martin, G.B., and Stebbins, C.E. (2006). A bacterial inhibitor of host programmed cell death defenses is an E3 ubiquitin ligase. *Science* **311**, 222–226.
25. Collier, S.M., Hamel, L.P., and Moffett, P. (2011). Cell death mediated by the N-terminal domains of a unique and highly conserved class of NB-LRR protein. *Mol. Plant Microbe Interact.* **24**, 918–931.
26. Bonardi, V., Tang, S., Stallmann, A., Roberts, M., Cherkis, K., and Dangl, J.L. (2011). Expanded functions for a family of plant intracellular immune receptors beyond specific recognition of pathogen effectors. *Proc. Natl. Acad. Sci. USA* **108**, 16463–16468.
27. Dong, O.X., Tong, M., Bonardi, V., El Kasmí, F., Woloshen, V., Wunsch, L.K., Dangl, J.L., and Li, X. (2016). TNL-mediated immunity in Arabidopsis requires complex regulation of the redundant ADR1 gene family. *New Phytol.* **210**, 960–973.
28. van Wersch, R., Li, X., and Zhang, Y. (2016). Mighty dwarfs: Arabidopsis autoimmune mutants and their usages in genetic dissection of plant immunity. *Front. Plant Sci.* **7**, 1717.
29. Cui, H., Gobbato, E., Kracher, B., Qiu, J., Bautor, J., and Parker, J.E. (2017). A core function of EDS1 with PAD4 is to protect the salicylic acid defense sector in Arabidopsis immunity. *New Phytol.* **213**, 1802–1817.
30. Van de Weyer, A.L., Monteiro, F., Furzer, O.J., Nishimura, M.T., Cevik, V., Witek, K., Jones, J.D.G., Dangl, J.L., Weigel, D., and Bemm, F. (2019). A species-wide inventory of NLR genes and alleles in Arabidopsis thaliana. *Cell* **178**, 1260–1272.e14.
31. Yang, S., and Hua, J. (2004). A haplotype-specific resistance gene regulated by BONZAI1 mediates temperature-dependent growth control in Arabidopsis. *Plant Cell* **16**, 1060–1071.
32. Cheng, Y.T., Li, Y., Huang, S., Huang, Y., Dong, X., Zhang, Y., and Li, X. (2011). Stability of plant immune-receptor resistance proteins is controlled by SKP1-CULLIN1-F-box (SCF)-mediated protein degradation. *Proc. Natl. Acad. Sci. USA* **108**, 14694–14699.
33. Wang, J., Hu, M., Wang, J., Qi, J., Han, Z., Wang, G., Qi, Y., Wang, H.W., Zhou, J.M., and Chai, J. (2019). Reconstitution and structure of a plant NLR resistosome conferring immunity. *Science* **364**, eaav5870.
34. Wang, J., Wang, J., Hu, M., Wu, S., Qi, J., Wang, G., Han, Z., Qi, Y., Gao, N., Wang, H.W., et al. (2019). Ligand-triggered allosteric ADP release primes a plant NLR complex. *Science* **364**, eaav5868.
35. Martin, R., Qi, T., Zhang, H., Liu, F., King, M., Toth, C., Nogales, E., and Staskawicz, B.J. (2020). Structure of the activated ROQ1 resistosome directly recognizing the pathogen effector XopQ. *Science* **370**. <https://doi.org/10.1126/science.abd9993>.
36. Ma, S., Lapin, D., Liu, L., Sun, Y., Song, W., Zhang, X., Logemann, E., Yu, D., Wang, J., Jirschtzka, J., et al. (2020). Direct pathogen-induced assembly of an NLR immune receptor complex to form a holoenzyme. *Science* **370**. <https://doi.org/10.1126/science.abe3069>.
37. Wang, W., Liu, N., Gao, C., Rui, L., and Tang, D. (2019). The Pseudomonas syringae effector AvrPtoB associates with and ubiquitinates Arabidopsis Exocyst Subunit EXO70B1. *Front. Plant Sci.* **10**, 1027.
38. Abramovitch, R.B., Kim, Y.J., Chen, S., Dickman, M.B., and Martin, G.B. (2003). Pseudomonas type III effector AvrPtoB induces plant disease susceptibility by inhibition of host programmed cell death. *EMBO J.* **22**, 60–69.
39. Wei, H.L., and Collmer, A. (2018). Defining essential processes in plant pathogenesis with Pseudomonas syringae pv. tomato DC3000 disarmed polymutants and a subset of key type III effectors. *Mol. Plant Pathol.* **19**, 1779–1794.
40. Chen, H., Chen, J., Li, M., Chang, M., Xu, K., Shang, Z., Zhao, Y., Palmer, I., Zhang, Y., McGill, J., et al. (2017). A bacterial type III effector targets the master regulator of salicylic acid signaling, NPR1, to subvert plant immunity. *Cell Host Microbe* **22**, 777–788.e7.
41. Deslandes, L., and Rivas, S. (2012). Catch me if you can: bacterial effectors and plant targets. *Trends Plant Sci.* **17**, 644–655.
42. Weßling, R., Epple, P., Altmann, S., He, Y., Yang, L., Henz, S.R., McDonald, N., Wiley, K., Bader, K.C., Gläßer, C., et al. (2014). Convergent targeting of a common host protein-network by pathogen effectors from three kingdoms of life. *Cell Host Microbe* **16**, 364–375.
43. Wang, Z., Yang, L., and Hua, J. (2023). The intracellular immune receptor like gene SNC1 is an enhancer of effector-triggered immunity in Arabidopsis. *Plant Physiol.* **191**, 874–884.
44. Saile, S.C., Jacob, P., Castel, B., Jubic, L.M., Salas-González, I., Bäcker, M., Jones, J.D.G., Dangl, J.L., and El Kasmí, F. (2020). Two unequally redundant “helper” immune receptor families mediate Arabidopsis thaliana intracellular “sensor” immune receptor functions. *PLoS Biol.* **18**, e3000783.
45. Mucyn, T.S., Clemente, A., Andriotis, V.M.E., Balmuth, A.L., Oldroyd, G.E.D., Staskawicz, B.J., and Rathjen, J.P. (2006). The tomato NBARC-LRR protein Prf interacts with Pto kinase in vivo to regulate specific plant immunity. *Plant Cell* **18**, 2792–2806.
46. Mathieu, J., Schwizer, S., and Martin, G.B. (2014). Pto kinase binds two domains of AvrPtoB and its proximity to the effector E3 ligase determines if it evades degradation and activates plant immunity. *PLoS Pathog.* **10**, e1004227.
47. Tamura, K., Stecher, G., Peterson, D., Filipowski, A., and Kumar, S. (2013). MEGA6: molecular evolutionary genetics analysis version 6.0. *Mol. Biol. Evol.* **30**, 2725–2729.

48. Waterhouse, A.M., Procter, J.B., Martin, D.M.A., Clamp, M., and Barton, G.J. (2009). Jalview version 2—a multiple sequence alignment editor and analysis workbench. *Bioinformatics* 25, 1189–1191.
49. Shimada, T.L., Shimada, T., and Hara-Nishimura, I. (2010). A rapid and non-destructive screenable marker, FAST, for identifying transformed seeds of *Arabidopsis thaliana*. *Plant J.* 67, 519–528.
50. Wang, Z.P., Xing, H.L., Dong, L., Zhang, H.Y., Han, C.Y., Wang, X.C., and Chen, Q.J. (2015). Egg cell-specific promoter-controlled CRISPR/Cas9 efficiently generates homozygous mutants for multiple target genes in *Arabidopsis* in a single generation. *Genome Biol.* 16, 144.
51. Lemoine, F., Correia, D., Lefort, V., Doppelt-Azeroual, O., Mareuil, F., Cohen-Boulakia, S., and Gascuel, O. (2019). NGPhylogeny.fr: new generation phylogenetic services for non-specialists. *Nucleic Acids Res.* 47, W260–W265.
52. Crooks, G.E., Hon, G., Chandonia, J.M., and Brenner, S.E. (2004). WebLogo: a sequence logo generator. *Genome Res.* 14, 1188–1190.
53. Clough, S.J., and Bent, A.F. (1998). Floral dip: a simplified method for *Agrobacterium*-mediated transformation of *Arabidopsis thaliana*. *Plant J.* 16, 735–743.
54. Ishiga, Y., Ishiga, T., Uppalapati, S.R., and Mysore, K.S. (2011). *Arabidopsis* seedling flood-inoculation technique: a rapid and reliable assay for studying plant-bacterial interactions. *Plant Methods* 7, 32.
55. Na Ayutthaya, P.P., Lundberg, D., Weigel, D., and Li, L. (2020). Blue native polyacrylamide gel electrophoresis (BN-PAGE) for the analysis of protein oligomers in plants. *Curr. Protoc. Plant Biol.* 5, e20107.

STAR★METHODS

KEY RESOURCES TABLE

REAGENT or RESOURCE	SOURCE	IDENTIFIER
<b>Antibodies</b>		
Mouse monoclonal anti-GFP	ABclonal, Inc. Wuhan, China	Cat#AE012; RRID: AB_2770402
Mouse monoclonal anti-GST	ABclonal, Inc. Wuhan, China	Cat#AE001; RRID: AB_2770403
Mouse monoclonal anti-MBP	ABclonal, Inc. Wuhan, China	Cat#AE016; RRID: AB_2770406
Mouse monoclonal anti-Ubiquitin	EASYBIO, Beijing, China	Cat#BE4002
Mouse anti-FLAG® M2-Peroxidase (HRP)	Sigma-Aldrich, MO, USA	Cat#A8592; RRID: AB_439702
Mouse monoclonal Anti-HA-Peroxidase	Roche	Cat#12013819001; RRID: AB_390917
Streptavidin HRP	BD Bioscience, NJ, USA	Cat#554066; RRID: AB_2868972
<b>Bacterial strains</b>		
<i>Agrobacterium tumefaciens</i> GV3101	Lab stock	N/A
<i>Escherichia coli</i> DH5a	Lab stock	N/A
<i>Escherichia coli</i> BL21	Lab stock	N/A
<i>Pseudomonas syringae</i> pv tomato (Pst) DC3000	Lab stock	N/A
<i>Pseudomonas syringae</i> pv tomato (Pst) DC3000 $\Delta$ avrPto	Lab stock from Jun Liu, CAU, Beijing, China	N/A
<i>Pseudomonas syringae</i> pv tomato (Pst) DC3000 $\Delta$ avrPto $\Delta$ avrPtoB	Lab stock of Wenxian Sun, CAU, Beijing, China	N/A
<i>Pseudomonas syringae</i> pv tomato (Pst) DC3000D36E	Wei et al. <sup>19</sup>	N/A
<i>Pseudomonas syringae</i> pv tomato (Pst) DC3000 D36E pME6012	This paper	N/A
<i>Pseudomonas syringae</i> pv tomato (Pst) DC3000 D36E pME6012 avrPtoB	This paper	N/A
<i>Pseudomonas syringae</i> pv tomato (Pst) DC3000 D36E pME6012 avrPtoB <sup>F173A/F479A</sup>	This paper	N/A
<b>Chemicals, peptides, and recombinant proteins</b>		
3 X FLAG peptide	Sigma-Aldrich, MO, USA	Cat#F4799
DTT	Solarbio Life Science, Beijing, China	Cat#D8220
Bafilomycin A1	MedChemExpress	Cat#HY-100558
Protease Inhibitor Cocktail Tablets	Roche	Cat#4693116001
<b>Critical commercial assays</b>		
Ni-NTA Agarose (affinity gel)	QIAGEN, Venlo, Netherlands	Cat#30210
Glutathione Sepharose 4B	GE Healthcare, IL, USA	Cat#17075601
Anti-GFP Nanobody Magarose Beads	KangTi Life Technology, Shenzhen, China	Cat#KTSM1334
Anti-HA Nanobody Magarose Beads	KangTi Life Technology, Shenzhen, China	Cat#KTSM1335
ANTI-FLAG® M2 Magnetic Beads	Sigma-Aldrich, MO, USA	Cat# M8823
Amylose Resin	New England BioLabs	Cat# E8021
ClonExpress MultiS One Step Cloning Kit	Vazyme, Nanjing, China	Cat#C113
ClonExpress II One Step Cloning Kit	Vazyme, Nanjing, China	Cat#C112
BlueNative PAGE System	Invitrogen, CA, USA	Cat#BN2001-2008

(Continued on next page)

Continued

REAGENT or RESOURCE	SOURCE	IDENTIFIER
Deposited Data		
Original data for generating the figures and supplemental figures in this manuscript	Mendeley Data	<a href="https://doi.org/10.17632/ph4y2sjbhc.1">https://doi.org/10.17632/ph4y2sjbhc.1</a>
Experimental models: Organisms/strains		
<i>A. thaliana adr1</i>	Lab stock	N/A
<i>A. thaliana adr1-L1 SAIL_302_C06</i>	Lab stock	N/A
<i>A. thaliana adr1-L2</i>	Lab stock	N/A
<i>A. thaliana pad4-1</i>	Lab stock	N/A
<i>A. thaliana sid2-2</i>	Lab stock	N/A
<i>A. thaliana ndr1-1</i>	Lab stock	N/A
<i>A. thaliana eds1-2</i>	Lab stock	N/A
<i>A. thaliana adr1/L1 (SAIL_302_C06)/L2</i>	Lab stock	N/A
<i>A. thaliana nrg triple</i>	Lab stock	N/A
<i>A. thaliana snc1-11</i>	Lab stock	N/A
<i>A. thaliana adr1-L1-c1 (Col-0)</i>	This paper	N/A
<i>A. thaliana adr1-L1-c2 (Col-0)</i>	This paper	N/A
<i>A. thaliana adr1-L1-c3 (Col-0)</i>	This paper	N/A
<i>A. thaliana adr1-L1-c4 (Col-0)</i>	This paper	N/A
<i>A. thaliana adr1-L1-c5 (SAIL_302_C06)</i>	This paper	N/A
<i>A. thaliana adr1-L1 (Ws-2)</i>	This paper	N/A
<i>A. thaliana adr1-L1(Col-0) X adr1-L1 (Ws-2) F<sub>2</sub></i>	This paper	N/A
<i>A. thaliana snc1-11 X adr1-L1-c1 (Col-0)</i>	This paper	N/A
<i>A. thaliana pad4-1 X adr1-L1-c1 (Col-0)</i>	This paper	N/A
<i>A. thaliana sid2-2 X adr1-L1-c1 (Col-0)</i>	This paper	N/A
<i>A. thaliana ndr1-1 X adr1-L1-c1 (Col-0)</i>	This paper	N/A
<i>A. thaliana eds1-2 X adr1-L1-c1 (Col-0)</i>	This paper	N/A
<i>A. thaliana adr1/L1 (Crispr)/L2 (Col-0)</i>	This paper	N/A
<i>A. thaliana adr1/L1 (Crispr) (Col-0)</i>	This paper	N/A
<i>A. thaliana adr1/L2 (Col-0)</i>	This paper	N/A
<i>A. thaliana L1 (Crispr) /L2 (Col-0)</i>	This paper	N/A
<i>A. thaliana pADR1-L1::ADR1-L1 (adr1-L1-c1)</i>	This paper	N/A
<i>A. thaliana pADR1-L1::ADR1-FLAG-TurboID (Col-0)</i>	This paper	N/A
<i>A. thaliana pADR1-L1::ADR1-L1-FLAG-TurboID (Col-0)</i>	This paper	N/A
<i>A. thaliana pADR1-L1::ADR1-L2-FLAG-TurboID (Col-0)</i>	This paper	N/A
<i>A. thaliana p35S::GFP-CC<sub>R</sub><sup>ADR1</sup> (adr1-L1-c1)</i>	This paper	N/A
<i>A. thaliana p35S::GFP-CC<sub>R</sub><sup>ADR1-L1</sup> (adr1-L1-c1)</i>	This paper	N/A
<i>A. thaliana p35S::GFP-CC<sub>R</sub><sup>ADR1-L2</sup> (adr1-L1-c1)</i>	This paper	N/A
<i>A. thaliana pSNC1::SNC1-HA (snc1-11 X adr1-L1-c1)</i>	This paper	N/A
<i>A. thaliana pSNC1::SNC1<sup>GK-AA</sup>-HA (snc1-11 X adr1-L1-c1)</i>	This paper	N/A
<i>A. thaliana pT-DNA::ADR1-L1<sup>Δ12aa</sup>-FLAG (adr1-L1-c5)</i>	This paper	N/A
<i>A. thaliana p35S::ADR1-L1<sup>Δ12aa</sup>-FLAG (adr1-L1-c5)</i>	This paper	N/A

Oligonucleotides

See Table S2

Recombinant DNA

pGEX-6P-1	Amersham Biosciences	27-4597-01
pCBCS nLUC	This paper	N/A

(Continued on next page)

**Continued**

REAGENT or RESOURCE	SOURCE	IDENTIFIER
pCBCS cLUC	This paper	N/A
pCBCS GFP-HA	This paper	N/A
pET1a MBP-mCherry	This paper	N/A
pCAMBIA 1300-ADR1-L1::ADR1-L1-FLAG	This paper	N/A
pCAMBIA 1300-ADR1-L1::ADR1-L1-FLAG-TurboID	This paper	N/A
pCAMBIA 1300-ADR1-L1::ADR1-L1-GFP	This paper	N/A
pCAMBIA 1300-ADR1-L1::ADR1-L1 <sup>D489V</sup> -GFP	This paper	N/A
pCAMBIA 1300-ADR1-L1::ADR1-L1 <sup>D489V</sup> -K34E/K48R-GFP	This paper	N/A
pCAMBIA 1300-35S::CC <sub>R</sub> <sup>ADR1-L1</sup> -GFP	This paper	N/A
pCAMBIA 1300-35S::CC <sub>R</sub> <sup>ADR1-L1</sup> -K34E/K48R-GFP	This paper	N/A
pCAMBIA 1300-ADR1::ADR1-FLAG	This paper	N/A
pCAMBIA 1300-ADR1::ADR1-FLAG-TurboID	This paper	N/A
pCAMBIA 1300-ADR1::ADR1-GFP	This paper	N/A
pCAMBIA 1300-ADR1::ADR1 <sup>D461V</sup> -GFP	This paper	N/A
pCAMBIA 1300-ADR1::ADR1 <sup>D461V</sup> -E35K/R49K-GFP	This paper	N/A
pCAMBIA 1300-35S::CC <sub>R</sub> <sup>ADR1</sup> -GFP	This paper	N/A
pCAMBIA 1300-35S::CC <sub>R</sub> <sup>ADR1</sup> -E35K-GFP	This paper	N/A
pCAMBIA 1300-35S::CC <sub>R</sub> <sup>ADR1</sup> -R49K-GFP	This paper	N/A
pCAMBIA 1300-35S::CC <sub>R</sub> <sup>ADR1</sup> -E35K/R49K-GFP	This paper	N/A
pCAMBIA 1300-35S::CC <sub>R</sub> <sup>ADR1</sup> (ADR1-L1 <sup>1-49aa</sup> )-GFP	This paper	N/A
pCAMBIA 1300-35S::CC <sub>R</sub> <sup>ADR1-L1</sup> (ADR1 <sup>1-50aa</sup> )-GFP	This paper	N/A
pCAMBIA 1300-ADR1-L2::ADR1-L2-FLAG	This paper	N/A
pCAMBIA 1300-ADR1-L2::ADR1-L2-FLAG-TurboID	This paper	N/A
pCAMBIA 1300-ADR1-L2::ADR1-L2-GFP	This paper	N/A
pCAMBIA 1300-ADR1-L2::ADR1-L2 <sup>D484V</sup> -GFP	This paper	N/A
pCAMBIA 1300-SNC1::SNC1-HA	This paper	N/A
pCAMBIA 1300-SNC1::SNC1 <sup>GK-AA</sup> -HA	This paper	N/A
pUC19-35S::SNC1-HA	This paper	N/A
pCBCS 35S::ADR1-FLAG-cLUC	This paper	N/A
pCBCS 35S::ADR1-L1-FLAG-cLUC	This paper	N/A
pCBCS 35S::ADR1-L2-FLAG-cLUC	This paper	N/A
pCBCS 35S::AvrPtoB-HA	This paper	N/A
pCBCS 35S::AvrPtoB <sup>F173A/F479A</sup> -HA	This paper	N/A
pCBNS 35S::GFP-CC <sub>R</sub> <sup>ADR1</sup>	This paper	N/A
pCBNS 35S::GFP-CC <sub>R</sub> <sup>ADR1-L1</sup>	This paper	N/A
pCBNS 35S::GFP-CC <sub>R</sub> <sup>ADR1-L2</sup>	This paper	N/A
pME6012 pKana::AvrPtoB-HA	This paper	N/A
pME6012 pKana::AvrPtoB <sup>F173A/F479A</sup> -HA	This paper	N/A
pCBCS 35S::AvrPtoB <sup>F173A/F479A</sup> -FLAG	This paper	N/A
pCBCS 35S::AvrPtoB-HA-nLUC	This paper	N/A
pET1a HIS-MBP-CC <sub>R</sub> <sup>ADR1</sup> -E35K/R49K	This paper	N/A
pET1a HIS-MBP-CC <sub>R</sub> <sup>ADR1</sup>	This paper	N/A
pET1a HIS-MBP-CC <sub>R</sub> <sup>ADR1-L1</sup>	This paper	N/A
pET1a HIS-MBP-CC <sub>R</sub> <sup>ADR1-L2</sup>	This paper	N/A
pGEX-6p-1-GST-AvrPtoB	This paper	N/A

(Continued on next page)

**Continued**

REAGENT or RESOURCE	SOURCE	IDENTIFIER
Software and algorithms		
MEGA6	Tamura et al. <sup>47</sup>	<a href="https://megasoftware.net">https://megasoftware.net</a>
Jalview	Waterhouse et al. <sup>48</sup>	<a href="https://www.jalview.org">https://www.jalview.org</a>
Graphpad Prism8	GraphPad Prism Software, Inc.	<a href="https://www.graphpad.com">https://www.graphpad.com</a>
Image J	National Institute of Health	<a href="http://imagej.nih.gov/ij">http://imagej.nih.gov/ij</a>

**RESOURCE AVAILABILITY**

**Lead contact**

Further information and requests for resources and reagents should be directed to and will be fulfilled by the lead contact, Wangsheng Zhu ([wangshengzhu@cau.edu.cn](mailto:wangshengzhu@cau.edu.cn)).

**Materials availability**

All requests for resources and reagents should be directed to the [lead contact](#) author. This study did not generate new unique reagents.

**Data and code availability**

This study analyses existing, publicly available data and does not generate new datasets and sequences. Information on the publicly available data is listed in the [key resources table](#). All data are provided in the main figures and supplemental figures. Original data have been deposited to Mendeley Data (<https://doi.org/10.17632/ph4y2sjbhc.1>): <https://data.mendeley.com/datasets/ph4y2sjbhc/1>.

**EXPERIMENTAL MODEL AND SUBJECT DETAILS**

**Arabidopsis**

*Arabidopsis thaliana* transgenic lines and mutants were derived from Col-0 unless *adr1-L1*<sup>W<sup>s</sup>-2</sup>. Plants were surface-sterilized with 75% (vol/vol) ethanol and 0.1% Tween 20 for 10 min, washed thoroughly in absolute ethanol for 3 min, then dried in an ultra-clean work bench before sown in soil or germinated on 1/2 MS solid medium (pH 5.7), and grown under long-day (16 h day/8 h night) or short-day (10 h day/14 h night) regimes at 23°C with relative humidity at 65%. Four-week-old plants were used for most experiments in this study. The *Arabidopsis* materials *eds1-2*, *pad4-1*, *eds1-2*, *sis2-2*, *nrg1 triple*, and *adr1 triple* were used in this study.

**Nicotiana benthamiana**

*N. benthamiana* plants were grown in a greenhouse at 23°C with long-day (16 h day/8 h night) conditions for 4-5 weeks.

**Bacterial Strains**

*Escherichia coli* and *Agrobacterium tumefaciens* (GV3101) were grown on LB (Lysogeny broth) plates or liquid media with appropriate antibiotic at 37°C and 28°C, respectively. *Pst* DC3000, *ΔavrPto* mutant, *ΔavrPto ΔavrPtoB* double mutant, DC3000 *ΔavrPto ΔavrPtoB* double mutant carrying *AvrPtoB*<sup>F173A/F479A</sup>, and *Pst* DC3000 D36E carrying *EV*, *AvrPtoB* and *AvrPtoB*<sup>F173A/F479A</sup> were grown at 28°C on the King's B (KB) medium with appropriate antibiotics.

**METHOD DETAILS**

**Cell death assays**

For the cell death assays, autoactive variants of ADR1s were co-expressed with indicated genes in *N. benthamiana* through agroinfiltration. Briefly, *Agrobacterium tumefaciens* GV3101 containing the relevant expression vectors were grown in liquid LB medium overnight in a shaking incubator (220 rpm, 28°C). *Agrobacteria* were precipitated through centrifugation and re-suspended in an infiltration buffer (10 mM MgCl<sub>2</sub>, 10 mM MES, pH 5.6). Vectors used for cell death assays are listed in [Table S1](#). For co-expression, each bacterial suspension was adjusted to the final OD<sub>600</sub> indicated in [Table S1](#), and infiltrated into 4-week-old *N. benthamiana* plants. The HR phenotypes were photographed and scored 2-3 days after agroinfiltration.

**Generation of transgene-free gene-edited lines**

The gRNA sequences for ADR1-L1 and ADR1-L2, which listed in [Table S2](#), were introduced to pREE401E, which was modified from an egg cell-specific CRISPR-CAS9 toolkit vector pHEE401E by adding Fast-RED selection marker,<sup>49,50</sup> to knock-out *ADR1-L1*. The

gene editing events were verified by PCR and Sanger sequencing. T<sub>2</sub> seeds that without red fluorescent seed coats were isolated as transgene-free seeds.

### Generation of high-order mutants

To generate high-order mutants, *adr1-L1-c1* was crossed with *pad4-1*, *sid2-2*, *eds1-2*, *nrg* triple, *adr1* triple. The homozygous high-order mutants were verified by PCR or Sanger sequencing. The genotyping primers are listed in [Table S1](#).

### RT-qPCR

RNA was extracted from plant tissue using an RNA isolation method (R401, Vazyme Biotech Co. Ltd., Nanjing, China). cDNA was synthesized from 0.5 μg high-quality total RNA (A260/A230>2.0 and A260/A280>1.8), using HiScript III First Strand cDNA Synthesis (R312, Vazyme Biotech Co. Ltd., Nanjing, China). SYBR master mix (Q711, Vazyme Biotech Co., Ltd., Nanjing, China) was used for quantitative real-time PCR in a Thermo Fisher system (ABI QuantStudio 6 Flex) according to the manufacturer's instructions. The comparative Ct (ΔΔCt) method was used to calculate the relative expression of genes of interest, using *ACTIN2* gene (*AT3G18780*) as an internal control. The primers used for qPCR are listed in [Table S2](#).

### Phylogeny analysis

To construct the phylogenetic tree of ADR1 homologs in angiosperms, the amino acid sequence of CC<sub>R</sub><sup>ADR1-L1</sup> was used as a query to BLAST in NCBI. The resulting sequences, which feature typical CC<sub>R</sub>, NB-ARC, and LRR domains, were used for further analysis. The MAFFT aligned sequences of the NB-ARC domain were used for phylogeny analysis with PhyML in NGPhylogeny.fr webserver.<sup>51</sup> Sequence LOGOs of ADR1, ADR1-L1, and ADR1-L2 in Brassicaceae were created by WebLOGO webserver<sup>52</sup> with grouped sequences according to phylogeny analysis results.

### Constructs and transgenic lines

The genomic fragments of *ADR1*, *ADR1-L1*, *ADR1-L2*, and *SNC1*, which contained native promoters, were amplified through PCR using Col-0 genomic DNA as the template. The resulting PCR products were cloned into entry vector pUC19 using homologous recombination (C115, Vazyme Biotech Co. Ltd., Nanjing, China) and transferred into the binary vector pCambia1300, which contains hygromycin marker for plant selection and various tags for protein detection. To generate *pT-DNA::ADR1-L1<sup>Δ12aa</sup>* and *p35S::ADR1-L1<sup>Δ12aa</sup>*, the truncated *ADR1-L1<sup>Δ12aa</sup>* CDS fragment was amplified from cDNA of *SAIL\_302\_C06*, and a 2 kb of T-DNA fragment near to insertion site and 35S *CaMV* fragment were amplified as promoters for *ADR1-L1<sup>Δ12aa</sup>*. The corresponding promoter and the *ADR1-L1<sup>Δ12aa</sup>* amplicon were cloned into pCambia1300 by multiple fragments homologous recombination. The CDS of CC<sub>R</sub><sup>ADR1s</sup> were amplified from Col-0 cDNA, cloned into the entry vector pUC19, and then subcloned into the binary vector pCBNS-GFP. The CDS of *AvrPtoB* was amplified using *Pst* DC3000 genomic DNA and cloned into pCBCS-HA/-FLAG and pME6012 by homologous recombination.

Site-directed mutagenesis and chimeric constructs were carried out by introducing corresponding changes in the primers using multiple fragments homologous recombination. Primer sequences used for domain swap and site-directed mutagenesis were listed in [Table S2](#).

The expression constructs were introduced into *Agrobacterium tumefaciens* GV3101 by electroporation. Stable transgenic plants were generated through the floral dipping method.<sup>53</sup> T<sub>1</sub> transformants were screened based on hygromycin selection or red fluorescent selection.

### TurboID based biotinylation in Arabidopsis seedling

Twenty-five 6-day-old TurboID transgenic seedlings grown on 1/2 Murashige and Skoog (MS) medium were submerged in 200 μM biotin solution for 6 hr. After the treatment, the seedlings were rapidly transferred to ice-cold ddH<sub>2</sub>O and washed three times, 1 minute each, and grounded with liquid nitrogen for protein extraction. The biotin treatment sample and buffer treatment (H<sub>2</sub>O) control were separated in 10% SDS-PAGE gel and followed by anti-FLAG and Streptavidin-HRP immunoblotting.

### Map-based cloning

To map the natural suppressor(s) of *adr1-L1* in *Ws-2*, a F<sub>2</sub> mapping population derived from a cross between *adr1-L1<sup>Ws-2</sup>* and *adr1-L1-c1* was generated. F<sub>2</sub> individuals with normal growth phenotypes were selected for genotyping. The SSLP markers were designed according to Yang's previous work,<sup>31</sup> and the detailed information is provided in [Table S2](#).

### Bacterial infection

For the bacterial infection assays on soil-grown plants in [Figure 4C](#), *Pst* DC3000 was precipitated by centrifugation and suspended in 10mM MgCl<sub>2</sub> solution. The concentrations were adjusted to OD<sub>600</sub> = 0.002, and were infiltrated into rosette leaves with a needleless syringe. Leaf discs (6 mm) from inoculated leaves were collected at 3 dpi for bacterial counts.

For the bacterial infection assays on germ-free plants in [Figure 6E](#), seedlings were grown on 1/2 MS medium in 90 x 90 mm culture plate for three weeks by the flood-inoculation.<sup>54</sup> Bacteria were grown overnight at 28°C in the KB medium plates with appropriate antibiotics. Bacteria were harvested from the plates, resuspended in sterile water with 0.025% Silwet L-77, and the concentration of *Pst* DC3000 *ΔavrPto* and *Pst* DC3000 *ΔavrPto ΔavrPtoB* were adjusted to an optical density at OD<sub>600</sub> = 0.02. 50 ml of bacterial

suspension was poured onto the culture plates containing 3-week-old plants and rested for 10 min at room temperature. After removing the bacterial suspension by decantation, the plates were sealed with 3M Micropore surgical tape and incubated at the growth chamber. The whole plant was weighed and collected at 2 dpi for bacterial counts.

### AvrPtoB-induced protein degradation in Arabidopsis

For the protein degradation assays, Arabidopsis plants were grown under short-day conditions. *Pseudomonas syringae* DC3000 D36E strains containing empty vector (EV), AvrPtoB, or AvrPtoB<sup>F173A/F479A</sup>, were cultured on solid KB (King's B) medium at 28°C for 24 h. Bacterial suspensions were adjusted to an OD<sub>600</sub> of 0.4 in 10 mM MgCl<sub>2</sub> solution, then infiltrated into 4-week-old Arabidopsis plants with a needleless syringe. Leaf discs at a diameter of 6 mm were collected from inoculated leaves at 0 hpi, 3 hpi, 6 hpi, and 12 hpi for immunoblots.

### Split-luciferase complementation assay

In the Split-Luc assays, AvrPtoB-nLuc was transiently co-expressed with ADR1-cLuc, ADR1-L1-cLuc, ADR1-L2-cLuc, and EV in 4-week-old *N. benthamiana* leaves. At 2 days post-infiltration (dpi) with *Agrobacterium* strains harboring the relevant constructs, leaves were infiltrated with 1 mM luciferin containing 0.02% Silwet L-77 and kept in the dark for 5 minutes before CCD imaging. To quantify the luciferase signal, leaf discs were collected from the inoculated leaves using a 6 mm puncher and placed into a 96-well plate with 60 μl H<sub>2</sub>O. 60 μl of 2 mM luciferin was added to the leaf discs in the 96-well plate before recording luminescence.

### Co-immunoprecipitation

*Agrobacterium* strains harboring AvrPtoB-HA, SNC1-HA, ADR1-FLAG, ADR1-L1-FLAG, and ADR1-L2-FLAG were grown overnight in LB medium containing appropriate antibiotics (220 rpm, 28°C) and used for agroinfiltration in *N. benthamiana*. Inoculated leaves were harvested 2dpi and ground into powder with liquid nitrogen. Ground tissues were homogenized in ice-cold extraction buffer (10% glycerol, 25 mM Tris-HCl pH 7.5, 1 mM EDTA, 150 mM NaCl, 2% PVP, 0.5% Triton-X100) supplemented with 1 mM DTT, anti-protease tablet (04693132001, Roche, USA). The resulting lysate was homogenized by mixing for 20 min on ice and centrifuged at 13000 rpm for 15 min at 4°C, with this step being repeated twice. The supernatant was incubated with 5 μl Antibodies-coupled beads (Anti-FLAG M2, M8823, Sigma-Aldrich, USA; Anti-GFP, KTSM1334, KangTi Life Technology, Shenzhen, China) for 3 hours at 4°C under gentle agitation. After incubation, beads were washed six times with washing buffer (25 mM Tris-HCl pH 7.5, 1 mM EDTA, 150 mM NaCl, 0.5% Triton-X 100, 1 mM DTT) at 4°C. SDS-loading buffer (8 M urea, 2% SDS, 20% glycerol, 100 mM Tris-HCl pH 6.8, 0.004% bromophenol blue) with 100 mM DTT was added to beads before boiling at 95°C for 5 min to release bound proteins. Released proteins were analyzed by immunoblots.

### In vitro ubiquitination assays

Bacteria (BL21) harboring GST-, MBP-6xHis-, and 6xHis- fusion protein expression vectors were cultured in LB at 37°C until an OD<sub>600</sub> of 0.6. Protein expression was induced by adding 0.4 mM IPTG and incubating at 16°C for 16 hours. Tagged proteins were purified separately using Glutathione Sepharose 4B (17075601, GE Healthcare, Chicago, USA) or Ni-NTA affinity agarose beads (30210, QIAGEN, Venlo, Netherlands).

Ubiquitination reactions were performed in a total volume of 30 μl, consisting of 50 mM Tris-HCl (pH 7.5), 2 mM ATP, 1 mM MgCl<sub>2</sub>, 1 mM DTT, 500 mg E1-His, 1 μg E2-His, 3 μg GST-AvrPtoB, 500ng MBP-CC<sub>RS</sub> and 3 μg ubiquitin for 8 h at 30 °C. Reactions were stopped by adding 30 μl SDS-loading buffer (8 M urea, 2% SDS, 20% glycerol, 100 mM Tris-HCl pH 6.8, 0.004% bromophenol blue) and the samples were boiled for 5 min at 95°C.

### In vitro pull-down assays

For the GST pull-down assays, 2 μg GST-tagged Protein, 20 μl Glutathione Sepharose 4B (17075601, GE Healthcare, Chicago, USA) and 10 μg MBP-6xHis-tagged protein were added to 1 ml pull-down buffer (50 mM Tris-HCl [pH 7.5], 200 mM NaCl, 0.5% [v/v] Triton X-100) and incubated for 4 hours under gentle rotation. Beads were washed 6 times with 1 ml pull-down buffer. SDS-loading buffers were added to beads before boiling to release bound proteins. The released proteins were analyzed by immunoblots using anti-Glutathione-S-Transferase (AE001, AbClonal, Wuhan, China) and anti-MBP (AE016, AbClonal, Wuhan, China) antibodies.

For the SNC1-GFP pull-down assays, ground *N. benthamiana* leaves transiently expressing SNC1-GFP were homogenized in extraction buffer containing 10% glycerol, 25 mM Tris-HCl pH 7.5, 1 mM EDTA, 150 mM NaCl, 2% PVP, 0.5% Triton-X 100, 1 mM DTT, and protease inhibitor. The resulting lysate was centrifuged and subjected for SNC1-GFP precipitation using anti-GFP magnetic beads (KTSM1334, KangTi Life Technology, Shenzhen, China). The anti-GFP magnetic beads were then aliquoted into 4 tubes containing 2 μg MBP-tagged protein in 1 ml buffer containing 25 mM Tris-HCl pH 7.5, 1 mM EDTA, 150 mM NaCl, and 0.5% Triton-X100, and incubated for 3 hours under gentle rotation. Beads are washed 6 times with 1 ml pull-down buffer. SDS-loading buffers were added to beads before boiling to release bound proteins. The released proteins were analyzed by immunoblots using anti-GFP (AE012, AbClonal, Wuhan, China) and anti-MBP (AE016, AbClonal, Wuhan, China) antibodies.

### Blue Native-PAGE

Blue native polyacrylamide gel electrophoresis (BN-PAGE) was performed according to Na Ayutthaya et al.<sup>55</sup> Three 14-day-old seedlings, infected with or without *Pst* D36E, were collected and homogenized in 1 x NativePAGE Sample Buffer (BN20032, Invitrogen,

CA, USA) supplemented with 1% n-dodecyl  $\beta$ -D-maltoside (DDM) and protease inhibitor cocktail (4693116001, Roche, USA). Homogenization was achieved by gently mixing on ice for 20 min, followed by 20000 g centrifugation for 15 min at 4°C. The resulting supernatant was mixed with 0.25% G-250 Sample Additive and loaded on a NativePAGE 3-12% Bis-Tris gel (BN1001BOX, Invitrogen, CA, USA) for electrophoresis.

#### QUANTIFICATION AND STATISTICAL ANALYSIS

In quantification experiments, the relative intensities of immunoblotting band were processed and quantified with Image J software. Statistical parameters are reported in the figures and figure legends. Statistical analysis was performed by GraphPad Prism 8 and Microsoft Office Excel 2019 in this work. Statistical significance between two groups were analyzed by two-tailed Student's t test, and two groups were analyzed by one way ANOVA or two ways ANOVA.